

学位論文

Functional analysis of retinoic acid in cardiac postnatal
maturation and regeneration.

(生後心臓成熟と心臓再生におけるレチノイン酸の機能解析)

平成 28 年度 12 月博士 (理学) 申請

東京大学大学院理学系研究科

生物科学専攻

伊藤航平

Contents

Abstract	2
General introduction	4
Mutant phenotype of retinoic acid synthetic enzymes	4
Retinoic acid synthesis and property	4
Function of retinoic acid in heart	4
Figures	5
Chapter 1 Fish heart regeneration and retinoic acid	7
1-1. Introduction	7
1-2. Materials and Methods	9
1-3. Results and Discussion	15
1-3-1. Medaka Heart Repair after Ventricular Resection.....	15
1-3-2. Cardiomyocyte Proliferation in the Medaka Heart	18
1-3-3. Expression Analysis of <i>fli1</i> after Ventricular Resection	19
1-3-4. Cloning of medaka periostin gene and its expression/ localization analysis.....	20
1-3-5. Phenotypes of <i>periostin-b</i> null mutants.....	23
1-3-6. <i>Raldh2</i> Analysis after Ventricular Resection.....	24
1-4. Figures	26
Chapter 2 Proliferation/ hypertrophy transition of neonatal cardiomyocytes and retinoic acid	41
2-1. Introduction	41
2-2. Materials and Methods	42
2-3. Results	45
2-3-1. CM proliferation and hypertrophy after birth.....	45
2-3-2. Transient upregulation of <i>Raldh2</i> in neonatal hearts.....	46
2-3-3. Transient increase of RA synthetic cells in neonatal hearts.....	47
2-3-4. Expression analysis of RA-relative genes.....	47
2-3-5. Cell type analysis of <i>Raldh2</i> ⁺ cells.....	48
2-3-6. <i>In vivo</i> effects of all-trans RA in neonatal mice.....	49
2-3-7. <i>In vivo</i> effects of RA synthetic inhibitor (DEAB) in neonatal mice.....	50
2-4. Discussion	51
2-5. Figures	53
Chapter 3 General conclusion	62
References	63
Acknowledgement	68

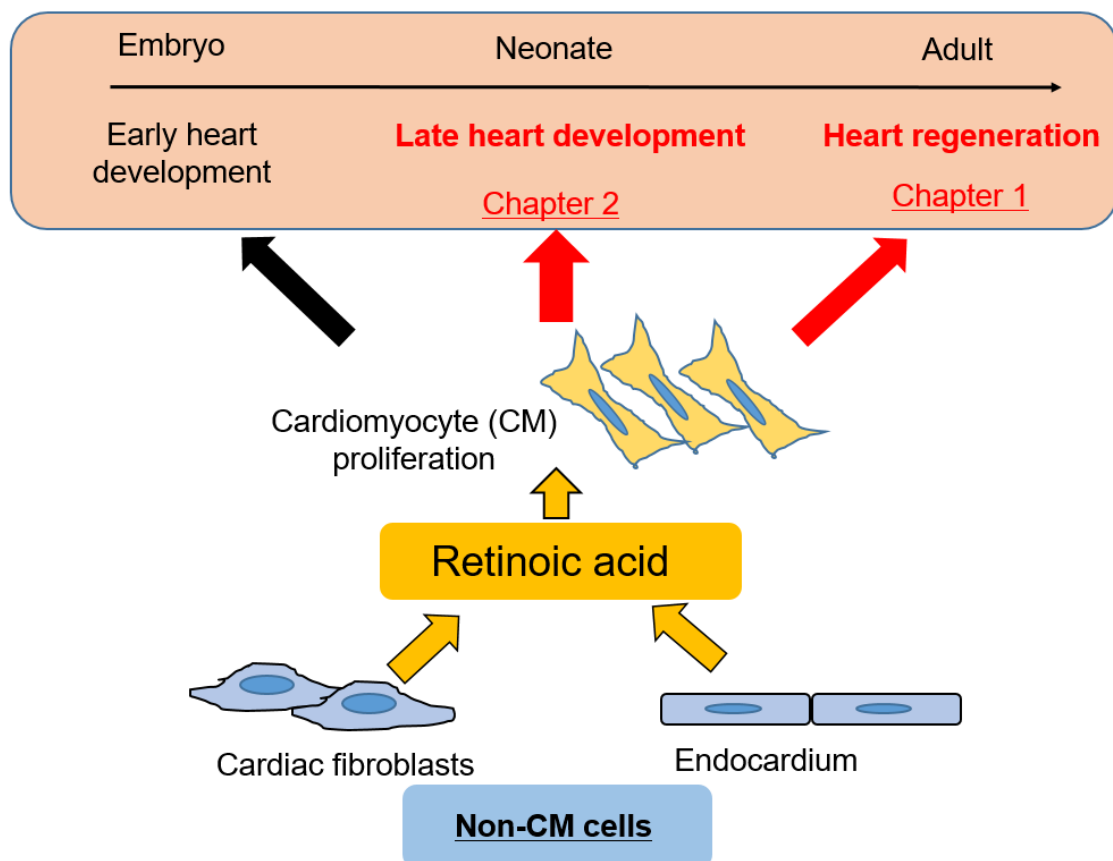
Abstract

The heart is an essential organ for living organism. A small defect in cardiac developmental process can cause abnormality of cardiac morphogenesis, leading to early lethality or serious cardiac dysfunction. Cardiac development continues after birth and cardiac maturation during the first 2 weeks of neonatal stages is an important process. At this stage, cardiomyocytes (CMs) stop their proliferation dramatically and initiate hypertrophy instead. The transition of CM from proliferation to hypertrophy is an irreversible process and determines the final number of CM in the heart, and an imbalance at this step can cause cardiac dysfunction. In addition to CM, non-CM cells in the heart such as cardiac fibroblasts are supposed to play roles in the maturational processes, and their functions have not been fully understood. Moreover, although a substantial change in CM property after birth is well known, the changes in non-CM cells after birth and their relationships to CM remain unknown.

Previous studies on heart regeneration using fish models have revealed that *Raldh2*, a gene encoding synthetic enzyme of retinoic acid (RA), is differentially expressed in endocardial cells in cardiac regenerative/ non-regenerative fish hearts. Their analysis suggested that non-CM cells contribute to CM proliferation during cardiac regeneration by producing RA, which is a well-known biologically active ligand that plays essential role for early embryonic heart development by facilitating CM proliferation. Furthermore, RA was shown to disturb CM hypertrophy *in vitro*. Thus, RA has multiple function in CM proliferation and hypertrophy. However, because *Raldh2* knockout mice are embryonic lethal around embryonic stage 10.5, RA functions at a late stage of cardiac development such as the neonatal maturation has not been known.

In this study, I show RA contribution to neonatal CM maturation. The *Raldh2* was transiently upregulated in cardiac fibroblasts during neonatal stages. The Raldh enzyme activity and RA-related gene expression were also upregulated. An excess of RA facilitated CM proliferation and accelerated heart growth. This study for the first time suggests that RA plays a role not only in cardiac development and regeneration but also in cardiac maturation by extending the time window of CM proliferation at neonatal stages. Further studies of cardiac maturation will contribute to understanding of cardiac disease and to medical application.

Graphical abstract



General introduction

Mutant phenotype of retinoic acid synthetic enzymes

Retinoic acid (RA), a derivative of vitamin A, is known to be essential for embryogenesis and mutations of main RA synthetic enzyme *Raldh2* (*Retinaldehyde dehydrogenase2*) can result in embryonic lethality around E10.5¹. *Raldh2*^{-/-} mutant hearts fail to undergo cardiac looping² and show reduced posterior chamber (atria and sinus venosus) outgrowth, and defective ventricular trabeculation¹. Furthermore, they show abnormality in forebrain and craniofacial development. *Raldh1* and *Raldh3* were also known as RA synthetic enzyme. *Raldh1*^{-/-} mutant is viable and shows no phenotype³. *Raldh3*^{-/-} mutant is also viable, but shows abnormal development of semicircular canals⁴.

Retinoic acid synthesis and property

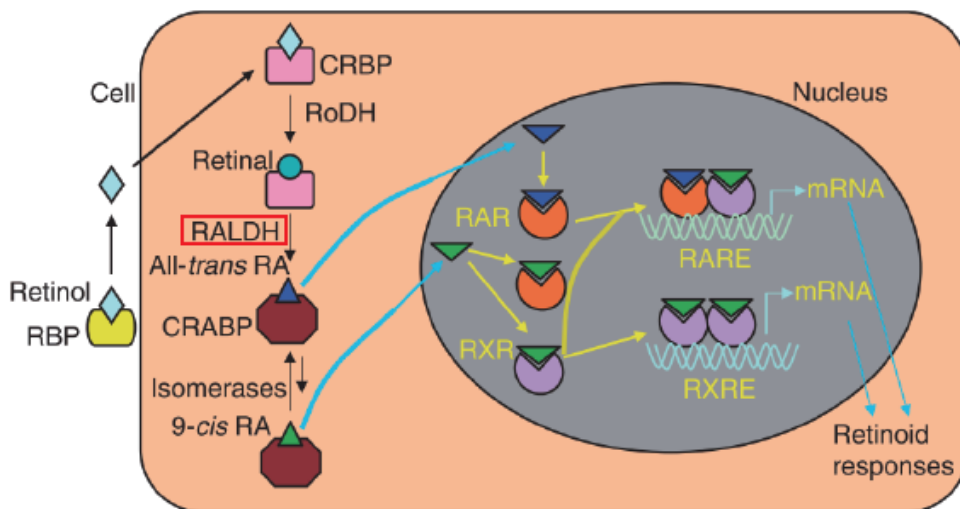
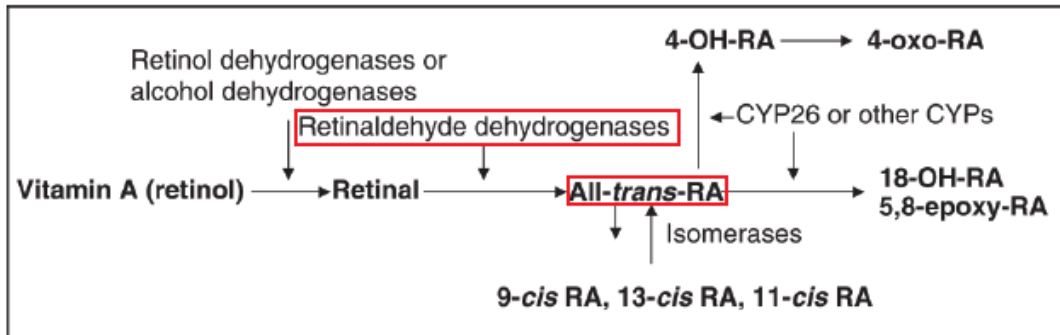
At the first step of RA synthesis, vitamin A (retinol) is uptaken from the blood stream and metabolized into retinal (Fig. 1). Retinal is metabolized into all-trans RA by *Raldh* enzymes. All-trans RA binds to Retinoic acid receptor (RAR) and works as a transcription factor in nucleus. RA is liposoluble and well-known as a diffusible morphogen.

Function of retinoic acid in heart

RA is known to repress CM hypertrophy *in vitro*⁵⁻⁷. Furthermore, RA signaling is indispensable for developmental cardiac morphogenesis and for the capacity to stimulate CM proliferation via fibroblast growth factor (FGF), erythropoietin (EPO), and insulin-like growth factor (IGF)⁸⁻¹⁰ signaling. RA is also known to stimulate CM proliferation in adult fish hearts, and RA signaling is essential for CM proliferation during zebrafish heart regeneration¹¹. Thus, RA is implicated in hypertrophy and proliferation of CM (Fig. 2). However, RA function in late stage of cardiac development and adult stage is not fully

understood. In this study, the author attempted to elucidate functions of retinoic acid in late stage of cardiac development and adult heart regeneration.

Figures



(Baker et al., 2007, Retinoic acid and the heart.)

Fig. 1. Pathways of retinoic acid (RA) synthesis.

Vitamin A (retinol) is uptaken from blood stream and metabolized into retinal at first. Retinal is metabolized into all-trans RA by RALDH (Retinaldehyde dehydrogenase). All-trans RA binds to Retinoic acid receptor (RAR) and works as a transcription factor in nucleus.

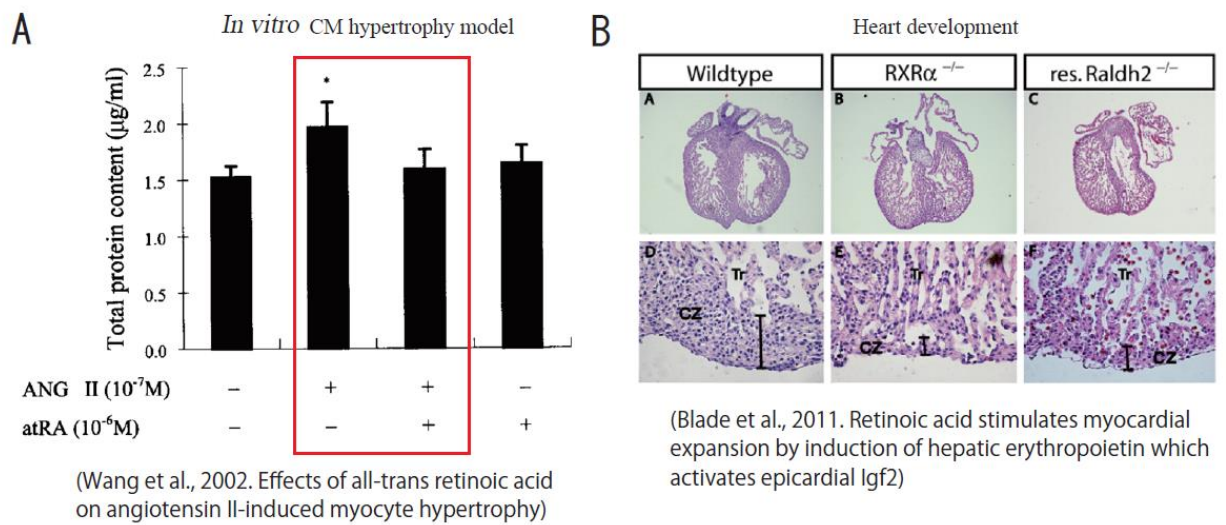


Fig. 2. Retinoic acid (RA) and CM hypertrophy/ CM proliferation

(A) RA suppresses Angiotensin II (hypertrophy inducer)-induced CM hypertrophy *in vitro*.

(B) Disturbance of RA signaling induces hypoplasia of compact zone muscle in cardiac development, which is indicative of suppressed CM proliferation.

Tr. trabecular muscle, CZ. compact zone muscle.

Chapter 1 Fish heart regeneration and retinoic acid

1-1. Introduction

Adult mammalian hearts do not regenerate after injury, which can be implicated in human heart diseases, including ischemic myocardial infarction and scar formation¹². In contrast to mammalian hearts, non-mammalian vertebrates such as fishes and amphibians have the ability to regenerate scarless hearts^{13,14} (Fig. 1-1), and this regenerative ability relies mainly on the proliferation of existing cardiomyocytes¹⁵⁻¹⁷ (Fig.1-2). Along with the infiltration of proliferating cardiomyocytes, the wound is highly vascularized with capillaries of coronary vessels^{18,19} (Fig.1-3).

In zebrafish heart regeneration, the importance of extracellular matrix (ECM) molecules such as fibronectin and tenascin-C have also been shown so far and these molecules are induced by TGF- β ^{20,21}. In the case of the healing process of mammalian hearts, another ECM molecule, periostin, is expressed and functions to promote the migration of cardiac fibroblasts and fibrillogenesis, leading to scar formation together with fibronectin and tenascin-C²²⁻²⁴. In humans, periostin is abundantly expressed in the infarct border after myocardial infarction; and its expression in mice is induced by TGF- β following inflammation at the infarct border²⁵. Periostin induces the migration of cardiac fibroblasts via integrin $\alpha v \beta 3$, which induces phosphorylation of the downstream kinase FAK (focal adhesion kinase) in these cells, leading to the production of type I collagen. Thereafter, periostin acts to promote collagen cross-linking in ECM. At later chronic stage of a myocardial infarction, fibrillogenesis is accelerated by periostin and proceeds to generate a tight scar, in a similar fashion as seen in cardiac hypertrophy²⁶.

Regarding the molecular events in zebrafish heart regeneration, injury to the heart initiates an organ-wide reaction detectable as the induced expression of *Raldh2*, a retinoic

acid synthesizing enzyme, in the endocardium as early as 3 hrs post-injury. This expression in the endocardium adjacent to regenerating cardiomyocytes remains active in the area of injury for several days. Disturbing the retinoic acid signaling induces decrease of cardiomyocyte proliferation during regeneration, indicative of the significance of retinoic acid (RA) signaling in zebrafish heart regeneration¹¹ (Fig. 1-4).

In spite of the growing interest in using fish models for probing heart regeneration, the difference in cardiac regenerative ability among fish species is unknown. Medaka is another representative fish animal model in addition to zebrafish; however, no reports on heart regeneration in medaka have been published, though the medaka fin does regenerate²⁷.

In this study, I examined the ability of medaka to regenerate the heart tissue after ventricular resection. Unexpectedly, I observed persistent collagen accumulation, mild proliferation of cardiomyocytes, a lack of vascularization, and the molecular marker expression patterns different from those of the zebrafish.

1-2. Materials and Methods

Fish Strains, Maintenance, and Surgery

The Cab²⁸ and Kaga^{29,30} medaka strains and the Ekkwill zebrafish strain (EkkWill Waterlife Resources) were used for this study. The latter was kindly donated by Dr. Kazu Kikuchi (Victor Chang Cardiac Research Institute). Adult fish were maintained at 28°C in a re-circulating system. Fish at >3 months of age were used in all experiments. Although ventricular apex amputation for both species was performed as previously described¹³, the ratio of excision area to total ventricular area was reduced for medaka survival. For medaka surgery, a sufficient supply of oxygen was needed for revival from the anesthesia. Experiments were carried out in accordance with the animal use guidelines at Tokyo Institute of Technology.

Histology

For optimization of staining conditions, the cryosection method was used with 14- μ m sections for AFOG staining, *fli1* analyses, *Raldh2* analyses, and periostin immunostaining of zebrafish; whereas for the medaka samples, the paraffin section method was used with 4- μ m sections for the EdU proliferation assay and 14- μ m ones for immunostaining. The AFOG staining was conducted as described previously¹³. Bright-field images were collected by an upright microscope (Carl Zeiss, Thornwood, NY; Axioplan2 imaging). Quantification of collagen-positive or ventricular area was performed by using Image J software. The ventricular area contained both ventricular myocardium and lumen.

For immunohistochemistry, the following primary antibodies were used: MF20 at 1:100 (Developmental Studies Hybridoma Bank [DSHB, Indianapolis, IN]), rabbit anti-collagen1 at 1:100 (AbD Serotec, 2150-1410), mouse anti-smooth muscle actin at 1:100

(Dako, Carpinteria, CA; M0851), rabbit anti-GFP at 1:500 (MBL, No. 598), rabbit anti-raldh2 at 1:500 (GeneTex, Irvine, CA; GTX124302), rabbit anti-zebrafish periostin-a at 1:100, rabbit anti-zebrafish periostin-b at 1:500, rabbit anti-medaka periostina at 1:100, and rabbit anti-medaka periostin-b at 1:100. The secondary antibodies used were goat anti-rabbit AlexaFluor 488 and goat anti-rabbit AlexaFluor 568, both at 1:500 (Molecular Probes, Eugene, OR).

The sections were treated with primary antibody overnight at 4 °C after preventing non-specific binding with Blocking One reagent (Nacalai Tesque), and then incubated with secondary antibodies 30 min at room temperature. For immunostaining with MF20 antibody, the antigen unmasking technique with citrate buffer was performed. The fluorescent images were collected by a laser-scanning confocal microscope (Olympus, Center Valley, PA; FV1000).

EdU Incorporation and Quantification

EdU treatment and staining were performed by using a Click-iT EdU Imaging Kit (Molecular Probes). EdU at 25 μ M in breeding water was incorporated into adult medaka over a 7-day period. The staining procedure conformed to the manufacturer's protocol. The fish were sacrificed after the last day of the treatment. Quantification of EdU⁺/MF20⁺ cells was carried out by using Image J software (NIH). For the area quantification, the outline of the ventricle was traced from the differential interference-contrast (DIC) image. As described above, the ventricular area contained both the ventricular myocardium and lumen. By utilizing the scale information, the area was determined. The mean cell counts and area quantification were performed by using 3 arbitrarily chosen sections per sample.

Generation of Medaka Transgenic Line

A fosmid clone (GOLWF no 683_j24) including the *Raldh2* gene, which was identified from the Medaka ensemble database, was used for homologous recombination. The homologous recombination was performed according to a previous report³¹. An EGFP-kanamycin cassette was amplified by using appropriate primers (5'-ATCAACAAAGCCATGACCGTCTCCACAGCCATGCAGGCCGGCACTGTCTGATGAGCCATATTCAACGGGA-3' [forward] and 5'-CTGGAAAATACACAGAGCATCGATCACTCTCGGTCATTAGACTCCTGCTCTTAGAAAACTCATCGAGCA-3' [reverse]) and recombined into the exon 1 of the medaka *Raldh2* gene. The recombined fosmid clone was injected into the cytoplasm of one-cell stage embryos. For establishment of *Raldh2-GFP* transgenic medaka, we used the fertilized eggs from the medaka Cab line.

The *fli1-GFP* transgenic line was kindly provided by Dr. M. Furutani-Seiki at the University of Bath, UK³².

Preparation of Rabbit Polyclonal Anti-Periostin Antibody

Polyclonal rabbit anti-medaka periostin-a/ periostin-b antibodies were raised by immunization of rabbits with keyhole limpet hemocyanin (KLH)-conjugated peptides DLLDPNEKLKLAENEN (representing amino acids 143–158 of medaka periostin-a) and ELLDEDVRNALVSNVN (representing amino acids 141–156 of medaka periostin-b). The antibodies were affinity purified with a minicolumn of HiTrap Protein G HP (GE Healthcare Biosciences, Waukesha, WI). Polyclonal rabbit anti-zebrafish periostin-a antibodies were raised by immunization of rabbits with KLHconjugated peptide EELDPASKAAVISRGN (representing amino acids 143–158 of zebrafish periostin-a)

and affinity purified by using a minicolumn of HiTrap NHS-activated HP (GE Healthcare Bio-sciences). The anti-zebrafish periostin polyclonal antibodies previously reported³³ were used as anti-zebrafish periostin-b antibodies.

Cloning of the Medaka Periostin Gene

As a template for cloning PCR, a mixed cDNA synthesized by RNA from whole ventricle was used. RNA extraction was performed by using ISOGEN (NIPPON GENE), and the cDNA synthesis was carried out with a PrimeScript II 1st strand cDNA synthesis Kit (Takara, Shiga, Japan). PCR products were cloned into pCR4-TOPO vector and sequenced. Specific primers designed for medaka periostin cloning were as follow:

Periostin-a: F- GCAGAGTGTGTTAGTGACCTT

R- TACCATGCACTTTGTCTACAG

Periostin-b: F- CTCTGGAAGTGGAAAGGCTTG

R- AGCAGGTAGCATGCAGTGAAG

Wholemout in situ Hybridization

Hearts were fixed overnight in 4% PFA and washed with PBST (1x PBS, 0.1% Tween20). Then hearts were dehydrated with 25%, 50%, 75% MeOH/ PBST series, and finally dehydrated in 100% MeOH overnight in -30°C.

(Day 1) The dehydrated hearts were re-hydrophilized with 75%, 50%, 25% MeOH/ PBST and PBST. After treatment of 10µg/ml proteinase K/ PBST and washing, hearts were re-fixed 20 minutes with 4% PFA at room temperature. Then washed with PBST, acetylation treatment was done with 0.1M Triethanolamine-HCl (pH 8.0) and 0.25% acetic anhydride/ 0.1 M triethanolamine-HCl (pH 8.0), to avoid non-specific electrostatic

binding between tissue and probes. Again washed with PBST, hearts were pre-hybridized 2 hour with hybridization buffer (50% formamide, 5x SSC, 0.1% Tween20, 50 µg/ ml heparin, 50 µg/ ml torula RNA) at 65 °C. Then the buffer was replaced with buffer containing 1µg/ ml of digoxigenin (DIG)-labeled antisense-RNA probes and incubated overnight at 65 °C.

(Day 2) Hearts were washed 2x 30 minutes with 50% formamide/ 2x SSC/ 0.1% Tween20, 15 minutes with 2x SSC/ Tween20 and 3x 30 minutes with 0.1x SSC/ 0.1% Tween20. Then washed with PBST at room temperature, hearts were blocked an hour with blocking buffer (5% lamb serum (GIBCO BRL), 200 µg/ ml of BSA/ PBST) at room temperature. The buffer was replaced with blocking buffer containing 1:4000 of alkaline phosphatase (AP)-labeled anti-DIG antibody and incubated overnight at 4 °C.

(Day 3) Hearts were washed with PBST sufficiently, then washed 2 times with AP reaction buffer (100 mM Tris-HCl pH 9.5, 50 mM MgCl₂, 100 mM NaCl, 0.1% Tween20, 1 mM Levamisole) at room temperature. The buffer was replaced with AP reaction buffer containing 450 µg/ml NBT, 175 µg/ml BCIP and incubated under blind condition until adequate coloring was observed. The coloring reaction was stopped with PBST washing, then fixed with 4% PFA/ PBS to preserve coloring. After washing, hearts were soaked in 80% glycerol and pictures were taken by using stereoscopic microscope (Leica, MZ16).

Semi-quantitative RT-PCR

Total RNA was extracted from 3 ventricles by using ISOGEN (NIPPON GENE). cDNA was synthesized from 1 µg total RNA by using PrimeScript II 1st. strand cDNA synthesis Kit (Takara). For PCR, cDNA was diluted into 1:20. Concentrations of each sample were adjusted by *β-actin* as an internal control. Primers used in PCR were as follows:

periostin-a F: GAAGAATGGCTTGGTTGTTCC

periostin-a R: CAGATGCAGCAGTAGCGAAAG

periostin-b F: TGTTGGACGAGGATGTGAGGA

periostin-b R: GTTTACAGTCACCACCCCATTGG

β -actin F: GATGACGCAGATCATGTTTGAG

β -actin R: AGATGGGTACTGTGTGGGTC

Generation of medaka *periostin-b* mutant by TILLING (Targeting Induced Local Lesions in Genomes) method and genotyping

TILLING is a method for mutant generation by using ENU, a chemical mutagen. Library of fish which have randomly mutated genomes was constructed at first. The library was screened by high-resolution melting temperature analysis for detection of fish with target mutation³⁴. The sperm of fish with *periostin-b* mutation was artificially fertilized to wild type egg³⁵ and the line was crossbred with wild type more than 6 generations to remove untargeted mutation. The established line has nonsense mutation in Tyr165 of medaka *periostin-b* amino acid sequence. Genotype of fish was checked by electrophoresis of enzymatically digested PCR products. Mse I restriction enzyme was used for the digestion. Primers used for PCR were as follows:

F- GATCGACCATGTTTACGGGAGC

R- GAAGACGTTTGTGGCCATGTG

Computational Analysis

Protein sequence alignment was performed by using GENETYX software ver.10 (GENETYX).

1-3. Results and Discussion

1-3-1. Medaka Heart Repair after Ventricular Resection

To examine the injury response of the medaka (*Oryzias latipes*) heart, I firstly established a method of operation to injure the medaka ventriculum. I adopted a ventricular apex resection model for injury of the myocardium. After the operation, the medaka appeared to be less active and more died than in the case of zebrafish. Therefore, I reduced the ratio of the excision area to total ventricular area so that a greater number of medaka would survive. The hearts collected from surviving medaka were observed at different time points by acid fuchsin orange G (AFOG) staining, to which collagen is sensitive (Fig. 1-5F–M). I also observed zebrafish (*Danio Rerio*) samples as a technical control (Fig. 1-5A–E). The ratio of excision area to total ventricular area was reduced to the same as for the medaka.

In the zebrafish, fibrin formation and collagen accumulation were observed at the wound site from 1 week to 2 weeks postamputation (Fig. 1-5B and C). The wound was filled with regenerated tissue, and little collagen remained by 30 days postamputation (dpa, Fig. 1-5D). At 60 dpa, zebrafish heart regeneration was nearly complete, and only faint staining of collagen remained (Fig. 1-5E).

In medaka, at 1 dpa, the injury area was filled with a blood clot (Fig. 1-5G), and then the clot was replaced with fibrin by 4 dpa (Fig. 1-5H). From 1 week to 2 weeks post-amputation, collagen accumulation was observed in the injured area (Fig. 1-5I and J). At 4 dpa, α -smooth muscle actin-positive putative myofibroblasts emerged in the wound area (Fig. 1-5K). Thus, the medaka heart showed a response similar to that of the zebrafish at these early time points. However, the wound in the medaka heart was occupied by dense collagen by 30 dpa (Fig. 1-5L). Furthermore, in medaka, the collagen scar remained

at 60 dpa (Fig. 1-5M) and even at 90 dpa (Fig. 1-6). At 14, 30, and 60 dpa, the collagen area gradually expanded rather than being reduced by absorption (Fig. 1-5N).

To investigate the cardiomyocyte contribution to wound healing in medaka, we performed co-immunostaining for cardiomyocytes and collagen at 30 dpa. Consistent with the AFOG staining results, collagen was detected, but no cardiomyocytes were observed in the injured area (Fig. 1-5O).

To explore whether these medaka heart phenotypes were strain-specific or not, the author confirmed these phenotypes in the heart of medaka strain Kaga²⁹, which has different genetic background from the Cab strain (Fig. 1-7). As a result, the Kaga strain also showed collagen scar in the injured heart at 30 dpa and it remained at 60 dpa, indicating that the long-term scar formation is common in medaka strains.

These results reveal that the medaka heart responded to an injury in a different manner compared with the zebrafish heart. The differential responses to injury in medaka and zebrafish may be explained by the following possibilities. One is that an excessive fibrotic response occurred in the medaka heart. This fibrotic response may be attributed to an excessive proliferation of and collagen production by fibroblastic cells such as myofibroblasts. Alternatively, matrix-degrading proteinases such as matrix metalloproteinases (MMPs), which are highly expressed in regenerating heart in zebrafish and newts^{20,36}, may not have been sufficiently activated in the injured medaka heart. A reduced collagen deposition is reported to facilitate myocyte progenitor engraftment to an infarcted heart³⁷. Therefore, in medaka, it is likely that the excessive collagen deposition disturbed the infiltration of cardiomyocytes into a wound and that repression of collagen deposition would have enhanced the infiltration by cardiomyocytes. The other possibility is that existing cardiomyocytes or cardiac progenitor cells in medaka remained

dormant or that perhaps the activation and proliferation of these cells was limited to a smaller population than in zebrafish, leading to the domination of fibrotic repair.

1-3-2. Cardiomyocyte Proliferation in the Medaka Heart

To examine the cardiomyocyte proliferation in the medaka heart after the injury, the author investigated DNA synthesis in medaka cardiomyocytes by EdU incorporation.

The author examined the proliferation during the period of 1–2 weeks post-amputation, as this is known to be the period of the peak proliferation of zebrafish cardiomyocytes following cardiac injury¹³. EdU was successfully incorporated into cardiac cells (Fig. 1-8A), and EdU⁺ cells were found in cardiomyocytes marked by the MF20 antibody, suggesting that cardiomyocytes were proliferating (Fig. 1-8B). However, there was no significant detectable difference between the numbers of double-positive cells in the two strains (Fig. 1-7C, 13 dpa). Taking the small injury size in this study into account, it is possible that the peak of proliferation was earlier than 1 week post amputation. Therefore, the author also quantified the proliferation at an earlier time point. However, no significant increase in cardiomyocyte proliferation could be detected at the end of the first week after amputation (Fig. 1-8C, 7 dpa).

Since EdU-incorporating cardiomyocytes were seen in uncut hearts, it is possible that renewal of cardiomyocytes may occur without injury. However, there was no quantitative difference between the uncut and injured hearts with respect to EdU-incorporating cardiomyocytes, suggesting that the proliferation of medaka cardiomyocytes/ progenitor cells remained at the base level or that their time of peak proliferation might be later than that of the zebrafish.

1-3-3. Expression Analysis of *fli1* after Ventricular Resection

Neovascularization seems to be essential for zebrafish heart regeneration^{18,38}. To examine vascular dynamics after injury in the medaka heart, the author investigated *fli1*-expressing cells by using a medaka *fli1-GFP* transgenic line. *Fli1* is the gene encoding the Ets family transcription factor Friend leukemia integration 1, a known marker for the vascular endothelium and endocardium^{39,40}. The author focused on 2 weeks post-amputation, when a highly vascularized wound is seen during zebrafish heart regeneration^{18,19}.

The endocardial and vascular endothelial cells in the heart of the *fli1-GFP* transgenic line showed GFP expression by anti-GFP antibody staining (Fig. 1-9A–D). GFP⁺ cells were not observed in the 4 and 7 dpa wound area (Fig. 1-9B, C, wo). Furthermore, no vascular cells were observed in the 14-dpa wound area (Fig. 1-9D).

In heart development, epicardial-mesenchymal transition (EMT) of the epicardium is important for formation of the coronary vasculature^{41,42}. Neovascularization after an injury is also likely to be mediated by epicardium-derived cells through EMT under the regulation of a growth factor such as FGF or PDGF in zebrafish^{18,19,43}. The results in this study may imply that the epicardium-derived cells failed to penetrate the wound and to form new vessel components in medaka. Furthermore, medaka does not have distinct coronary vessel structures in their heart, unlike zebrafish^{44,45}. Therefore, the medaka heart may not have the program to vascularize a heart injury de novo by epicardium-derived cells or by other cell populations.

1-3-4. Cloning of medaka periostin gene and its expression/ localization analysis

To examine the dynamics of ECM molecules after injury in zebrafish and medaka, the author focused on medaka periostin. At first, the author cloned two types of medaka *periostin* cDNAs which were termed *periostin-a* and *periostin-b*. The author sequenced them (Fig. 1-10B) and found that *periostin-b* was highly conserved between medaka and zebrafish (Fig. 1-10C).

Next, the author investigated the spatial expression pattern of medaka *periostin* after cardiac injury by whole-mount *in situ* hybridization (Fig. 1-11). In uncut heart, *periostin-a* was expressed in epicardium (Fig. 1-11D, arrowheads). After ventricular injury, the epicardial expression was augmented except for the injury area that the epicardium was removed by surgery (Fig. 1-11E). At 10 dpa, *periostin-a* was expressed in the injury area, suggesting the epicardium recovers and spreads over the surface of the injury (Fig. 1-11F). This transient decrease and recovery of *periostin-a* expression was confirmed by semi-quantitative PCR analysis (Fig. 1-11G).

As for medaka *periostin-b*, there was no expression in uncut hearts (Fig. 1-11K). However, *periostin-b* expression was detected along the amputation plane in the injury at 4 dpa (Fig. 1-11L). The expression was also seen at 10 dpa, and the signal was stronger than 4 dpa (Fig. 1-11M). These expression patterns after injury were confirmed by semi-quantitative PCR (Fig. 1-11N).

Because Periostin is a secreted ECM protein, there is a possibility that their localization is different from the *periostin*-expressing cells. Therefore, the author produced anti-medaka Periostin polyclonal antibodies based on amino acid sequences to investigate Periostin localization in injured hearts. The author also made anti-zebrafish Periostin-a

antibody for comparison between medaka and zebrafish. As for anti-zebrafish Periostin-b antibody, the reported one³³ was used.

Zebrafish Periostin-a localization was observed at atrio-ventricular valves and ventriculo-bulbal valves in the uncut heart (Fig. 1-12A). Although from 7 to 30 dpa, this Periostin type was not observed at the injured area (Fig. 1-12B-E), zebrafish Periostin-b was observed in the epicardium (Fig. 1-12F, arrowhead). In addition, it was detected within the blastema at 7 dpa (Fig. 1-12G); and furthermore, endocardial localization was also seen from 14 to 21 dpa (Fig. 1-12H-I, arrowhead). By 30 dpa, zebrafish Periostin-b localization was limited to the epicardium and not seen within the wound (Fig. 1-12J).

Medaka Periostin-a was detected in the epicardium and valves of the uncut heart (Fig. 1-12K, arrowhead). By ventricular apex resection, epicardial localization of Periostin-a was removed in the injured area (Fig. 1-12L). However, the epicardial localization revived gradually (Fig. 1-12M, arrowhead), and covered the wound from 21 to 30 dpa (Fig. 1-12N-O, arrowhead).

On the other hand, medaka Periostin-b was localized at the atrium (Fig. 1-12P, arrowhead) and valves (data not shown) in the uncut heart. After resection, this Periostin was detected in the border area of the wound (Fig. 1-12Q, arrowhead). Thereafter, the localization was seen in the wound (Fig. 1-12R-S, arrowhead), and remained within the wound at 30 dpa (Fig. 1-12T, arrowhead). These localization patterns of Periostin-a and Periostin-b were consistent with the expression pattern analysis (Fig. 1-11).

The zebrafish Periostin-b and the medaka Periostin-b were localized at the wound site in which the collagen deposition occurred. The coincidence of localization implies that zebrafish Periostin-b and medaka Periostin-b may function similarly in fibrillogenesis, which was previously reported as a function of Periostin²⁴. Periostin is known to behave

as a scaffold protein to generate the ECM structure together with fibronectin and tenascin-C²⁴. If that is the case, the repair of the medaka heart may be prolonged through fibrillogenesis promoted by this ECM structure, because medaka Periostin-b localization remained at the wound area in 30 dpa, whereas zebrafish Periostin-b was no longer localized at the wound area but detected in the epicardium 30 dpa.

1-3-5. Phenotypes of *periostin-b* null mutants.

The previous analysis revealed the difference of Periostin-b localization between zebrafish and medaka injured hearts (Fig. 1-12J, T). This result led the author to examine the effect of Periostin deficiency on the medaka heart. If the excessive fibrillogenesis by Periostin-b was suppressed, medaka hearts then could go to the regenerative direction. To test this hypothesis, the author generated *periostin-b* null medaka mutant by the TILLING method. The mutant has nonsense mutation in the first Fas I domain, which interacts with tenascin-C and integrins. The mutants developed and grew up normally, and there was no detectable abnormality in hearts. The author examined the reparative phenotype of the mutant hearts and compared with wild type hearts.

Surprisingly, the scar tissue formation in *periostin-b* mutant was substantially diminished compared with wild type (Fig. 1-13). Notably, collagen accumulation was hardly seen at 14 dpa (Fig. 1-13C) and was detectable but minimal at 60 dpa (Fig. 1-13D). However, a dent made by ventricular amputation was not restored, indicative of no CM supplementation to the injured area. These results suggest that suppression of ECM formation is not enough to induce regeneration in medaka hearts.

A recent study reported that the disturbance of ECM formation negatively affect zebrafish heart regeneration⁴⁶, suggesting significance of ECM as scaffold for regeneration. Therefore, the difference of cardiac regenerative capacity between medaka and zebrafish may be derived from other factors such as property of cardiomyocyte, rather than ECM formation.

1-3-6. *Raldh2* Analysis after Ventricular Resection

To examine the dynamics of the medaka endocardium after an injury, the author investigated the localization of retinoic acid in zebrafish and medaka by immunostaining with an anti-Raldh2 antibody. *Raldh2* is an enzyme responsible for synthesis of the morphogenetic factor retinoic acid (RA), which is essential for normal cardiac development and regeneration in the zebrafish heart^{11,47}. Because the anti-Raldh2 antibody did not work for immunostaining in the medaka heart, the author instead used the medaka *Raldh2-GFP* transgenic line.

In zebrafish, Raldh2 protein was observed in the epicardium but not detected in the endocardium in uncut heart (Fig. 1-14A). The endocardial Raldh2 was detected at 3 hours post amputation (hpa, Fig. 1-14B), as previously reported¹¹, and remained detectable at 2 weeks' post amputation (Fig. 1-14C-D, arrowhead).

In the medaka *Raldh2-GFP* transgenic line, the epicardium and valves gave green fluorescence of GFP, which was not seen in the endocardium, in uncut hearts (Fig. 1-14E). The GFP expression was not observed in the endocardium at 3 hpa (Fig. 1-14F). Furthermore, from 4 to 14 dpa, although a few fibroblast-like GFP-positive cells were detected within the myocardial tissues in medaka (Fig. 1-14G-H, arrowheads), there were no endocardial GFP-positive cells.

The expression pattern obtained from the analysis of the medaka *Raldh2-GFP* transgenic line resembled that of the *Raldh2* gene in the infarcted mouse heart, which lacks endocardial expression¹¹. Therefore, these results may imply that the medaka endocardium remained in an inactive state. Moreover, given that RA signaling is reported to be correlated with the proliferation of cardiomyocytes during zebrafish heart regeneration¹¹, the dormant state of the endocardium in medaka may implicate the

inability of cardiomyocyte proliferation because of the absence of RA signaling after injury.

In contrast to zebrafish heart regeneration, the data of medaka heart together suggest the possibility that the medaka could hardly regenerate heart tissues or that heart regeneration could be delayed. Considering the transient cardiac regenerative capacity of neonatal mice⁴⁸, medaka may also have a potential for heart regeneration in their early life. Therefore, a further study of the injury response in early time points will clarify a regenerative potential of medaka heart.

1-4. Figures

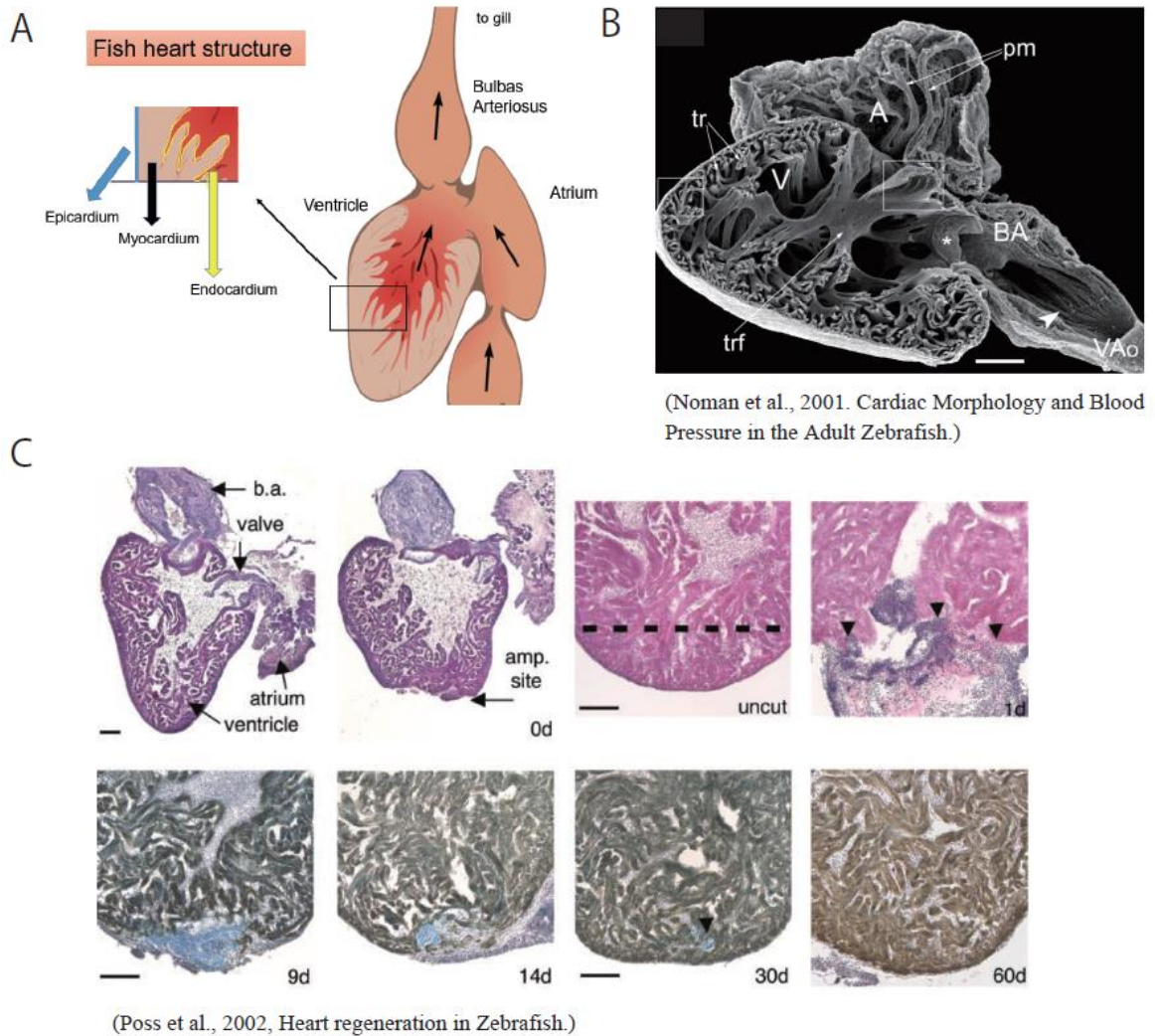
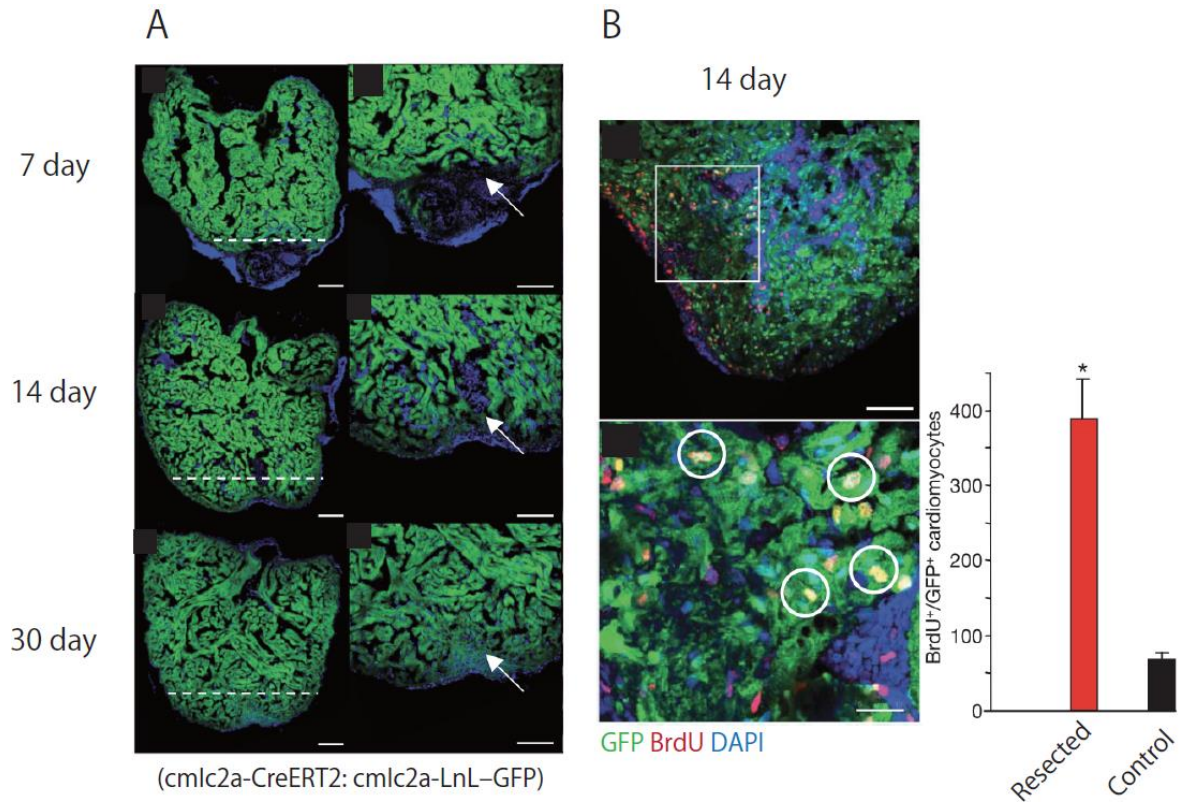


Fig. 1-1. Fish heart structure and zebrafish heart regeneration.

(A) Fish heart structure and cell components.

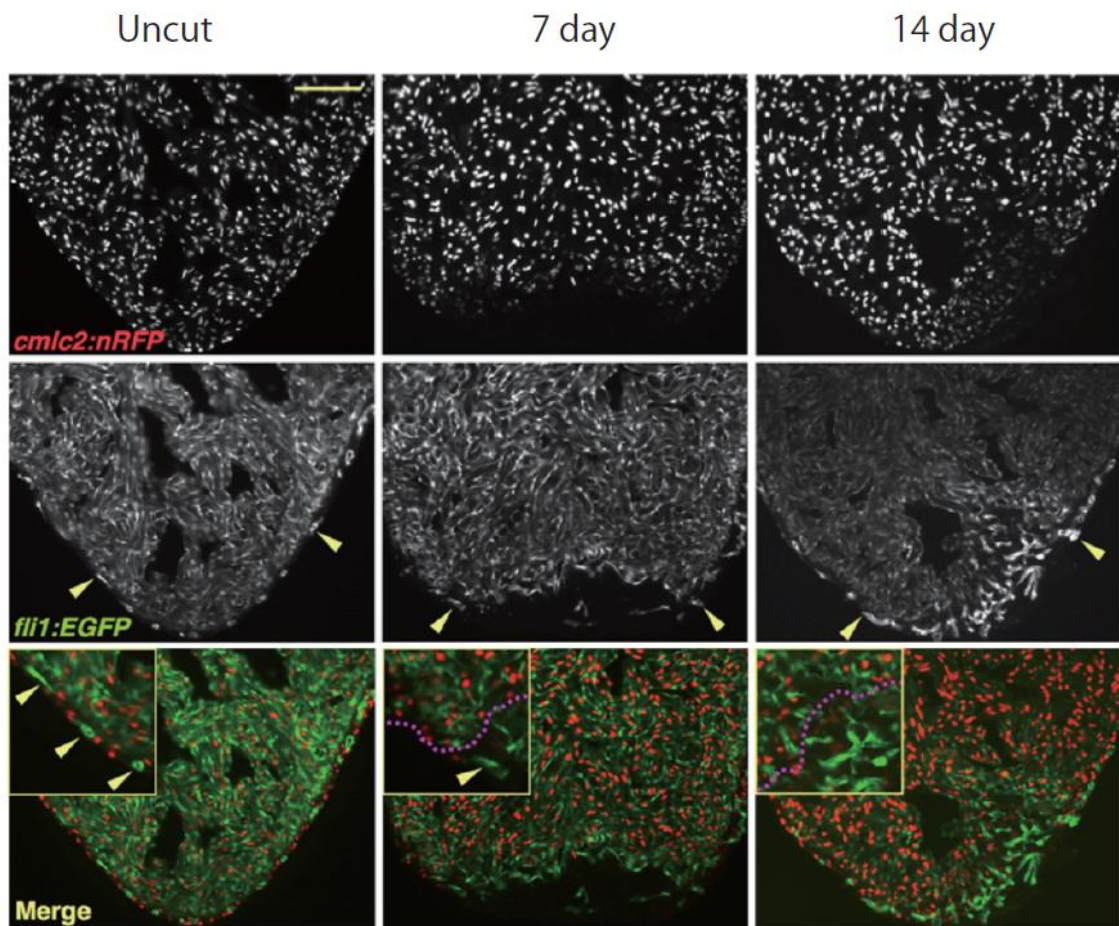
(B) Scanning electron microscopy (SEM) image of the saggital section of the adult zebrafish heart. A. atrium, BA. bulbus arteriosus, pm. pectinate muscle, tr. trabeculae, trf. trabecular fold, V. ventricle, VAo. ventral aorta.

(C) Heart regeneration in zebrafish. Zebrafish heart scarlessly regenerates after ventricular apex resection.



(Jopling et al., 2010, Zebrafish heart regeneration occurs by cardiomyocyte dedifferentiation and proliferation.)

Fig. 1-2. Contribution of existing cardiomyocytes to zebrafish heart regeneration.
 (A) GFP-labeled pre-existing cardiomyocytes occupied regenerated tissue after amputation.
cm1c2: cardiomyocyte marker.
 (B) Proliferation of GFP-labeled cardiomyocytes after 14 days post amputation.

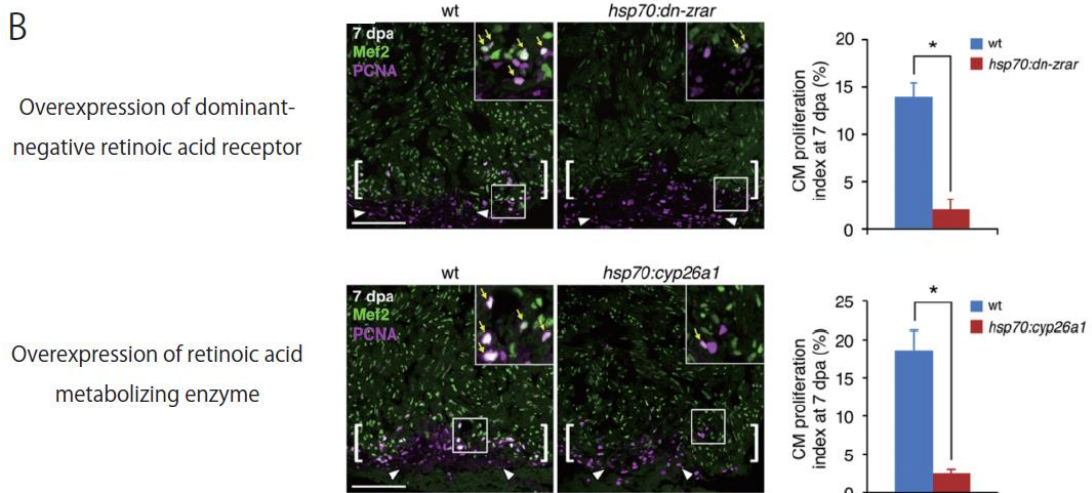
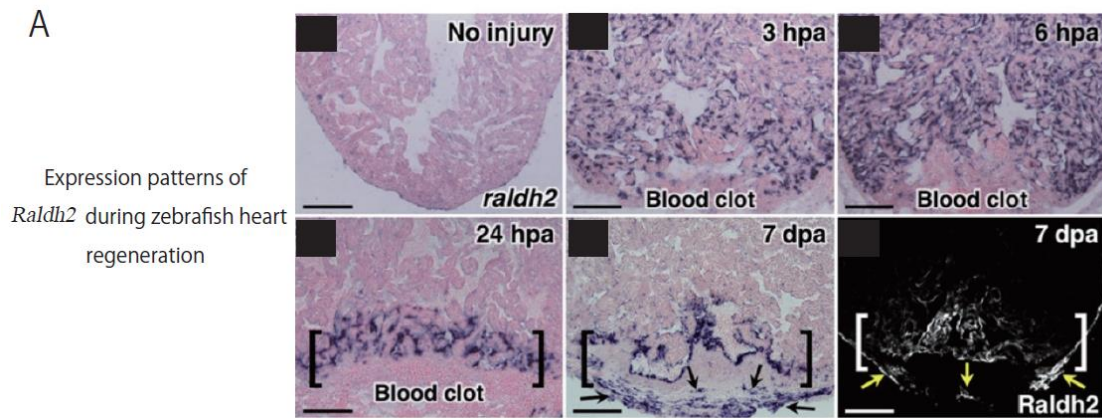


(Lepilina et al., 2006. A Dynamic Epicardial Injury Response Supports Progenitor Cell Activity during Zebrafish Heart Regeneration.)

Fig. 1-3. Neovascularization during zebrafish heart regeneration.

Vascular capillaries invade into injured area and contribute to regeneration.

cmlc2 : cardiomyocyte marker, *flil* : vascular endothelial cell marker



(Kikuchi et al., 2011. Retinoic Acid Production by Endocardium and Epicardium Is an Injury Response Essential for Zebrafish Heart Regeneration.)

Fig. 1-4. Retinoic acid signaling is essential for zebrafish heart regeneration.

(A) *Raldh2* is expressed during zebrafish heart regeneration.

(B) Disturbance of retinoic acid signaling decreases cardiomyocyte proliferation during regeneration.

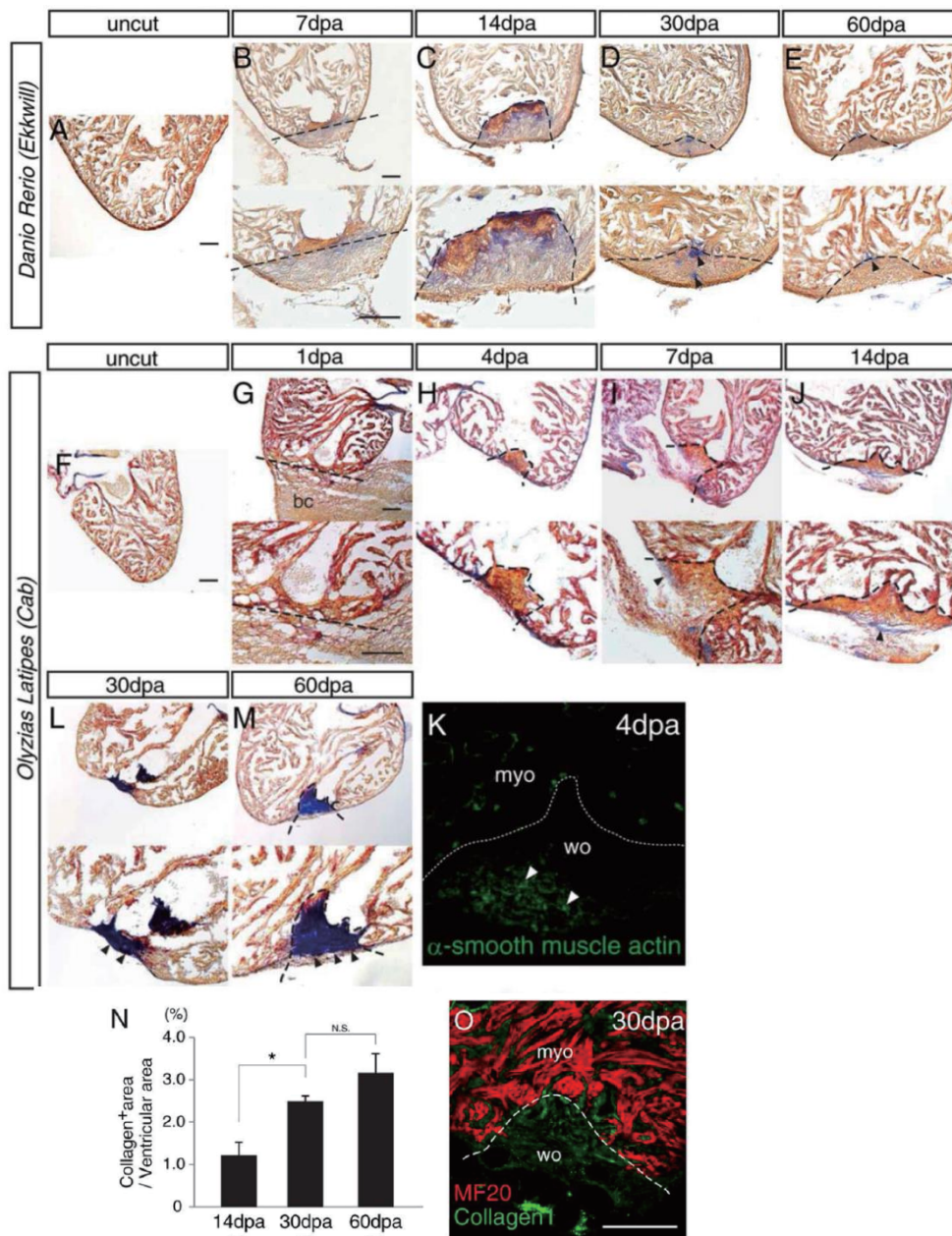


Fig. 1-5. Comparative analysis of the repair process in zebrafish and medaka hearts after ventricular resection.

A–L: Cryosections of fish hearts stained with AFOG (fibrin, orange; collagen, blue). A–E: Uncut (A) and injured Ekkwill zebrafish hearts (B–E). Fibrin tissues were observed at both 7 (B) and 14 dpa (C), but were absorbed by 30 dpa (D). Collagen was seen from 7 dpa (B) and then was mostly absorbed by 60 dpa (E). F–M: Uncut (F) and injured (G–M) Cab medaka hearts. A blood clot was seen at 1 dpa (G) and was replaced by fibrin by 4 dpa (H). The fibrin was absorbed by 30 dpa (L). Collagen began to accumulate from 7 dpa (I), and this accumulation increased thereafter (J, L, and M). Dense collagenous tissue covered the wound area by 60 dpa (M). Black arrowheads indicate collagen tissues. K: Immunohistochemistry with anti- α -smooth muscle actin antibodies at 4 dpa. White arrowheads indicate putative myofibroblasts. N: Quantification of collagen-positive area ratio indicates scar formation at 30 and 60 dpa. Student’s t-test, * $p < 0.05$. N.S., not significant. Numbers in parentheses indicate the sample number. O: Immunohistochemistry of MF20 for medaka cardiomyocytes and with anti-collagen I antibodies in the injured area at 30 dpa. The dashed line indicates the approximate injury border. bc, blood clot; myo, myocardium; wo, wound area. Scale bars = 100 μm .

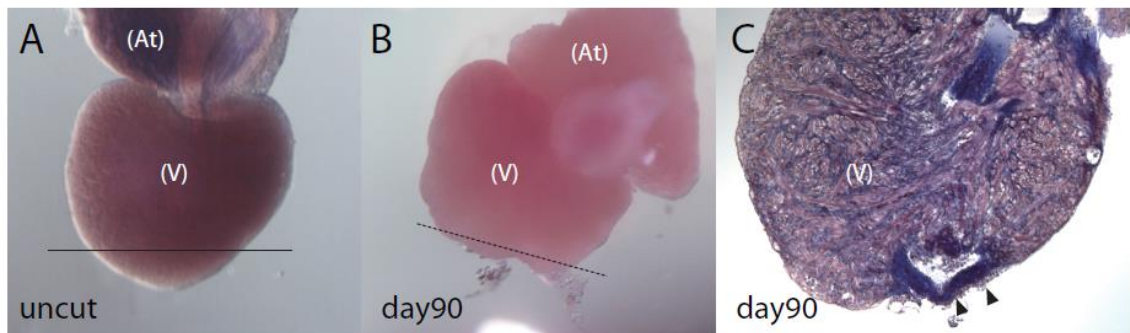
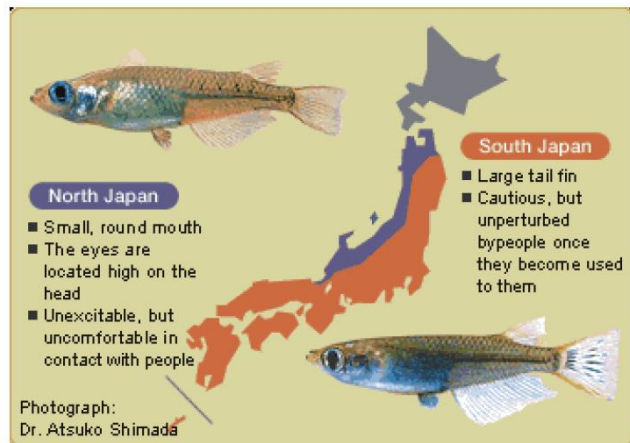


Fig. 1-6. Scar tissue remains in medaka heart at 90 days post injury. Wholemount view of uncut ventricle (A) and ventricle at 90 days post injury (B). (C) AFOG staining image of medaka heart at 90 days post injury. At. atrium, V. ventricle. Black dashed line indicates amputation line.

A



(Takeda, Biohistory Jyournal, Autumn, 2004.)

B

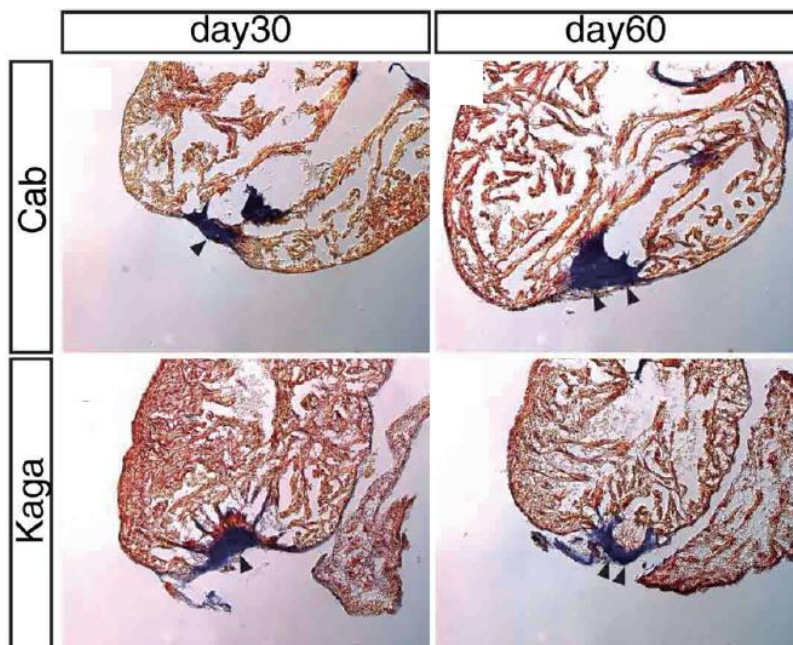


Fig. 1-7. Heart reparative phenotype in northern medaka strain, Kaga.

(A) Two distinct Japanese medaka populations. Cab belongs to the southern population and Kaga belongs to the northern population.

(B) Comparison of cardiac reparative phenotypes between Cab and Kaga strains by AFOG staining. Arrowheads indicate collagen scar.

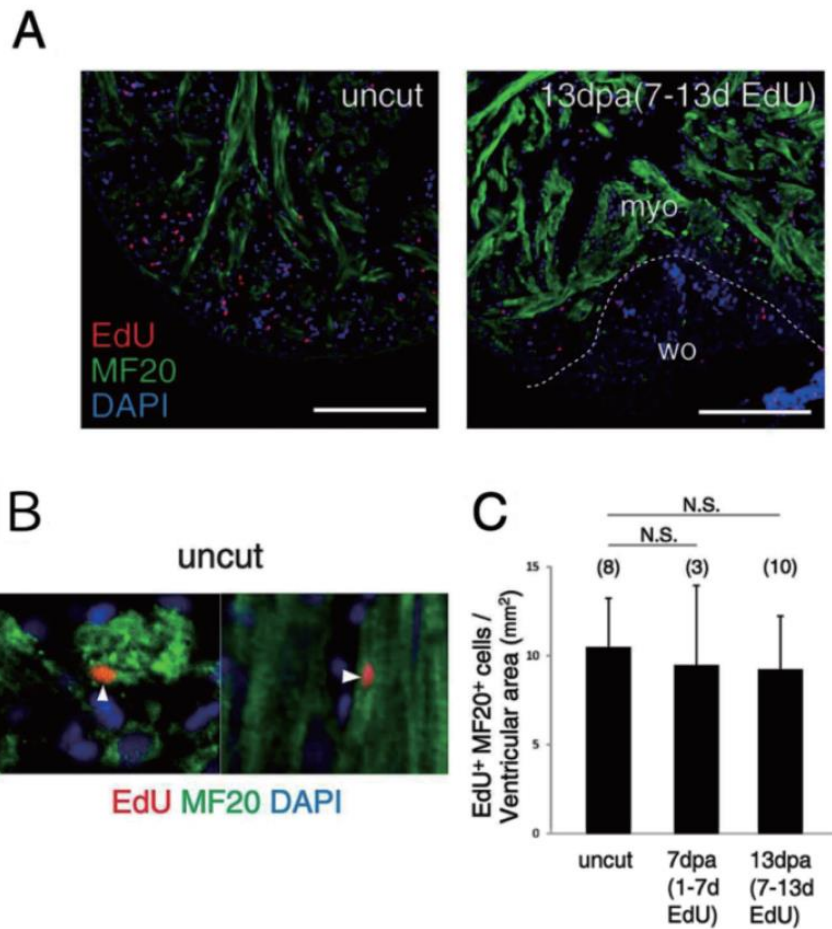


Fig. 1-8. Cardiomyocyte proliferation after ventricular resection.

(A) Fluorescent images of EdU/ MF20 double-stained hearts. EdU-incorporating uncut and resected (13 dpa) hearts are shown (EdU incorporated from 7 to 13 dpa).

(B) Representative EdU/ MF20 double-positive cardiomyocyte (arrowhead) in the uncut heart.

(C) Quantification of EdU/MF20 double-positive cells in the ventricle. The count was normalized by the ventricular area. Numbers in parentheses indicate the sample number. Student' s t-test, N.S., not significant. The dashed line indicates the approximate injury border. myo, myocardium; wo, wound area. Scale bars=100 μ m.

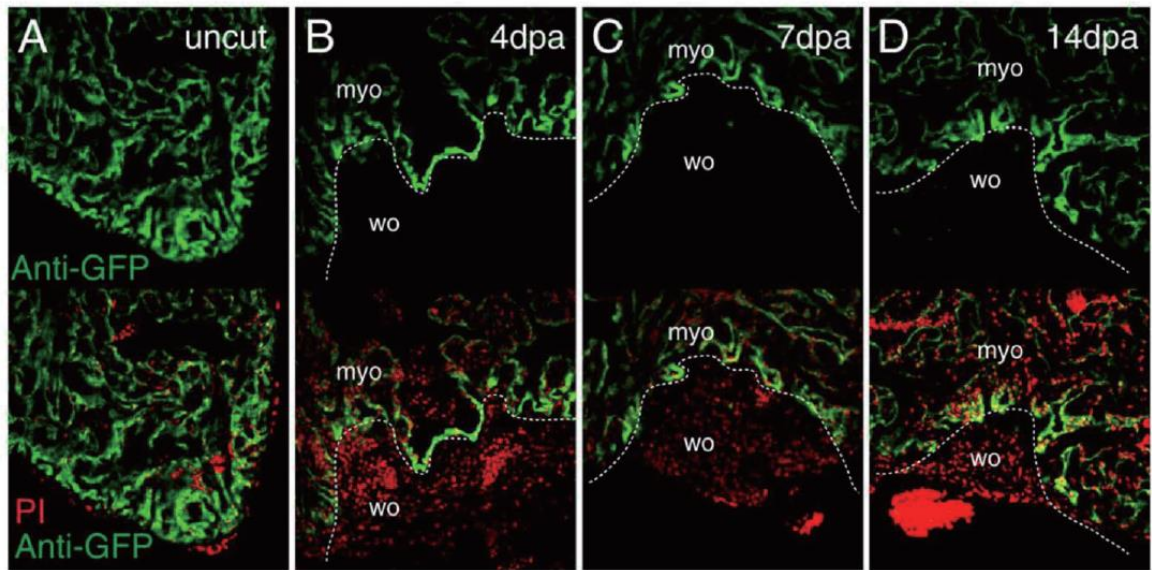


Fig. 1-9. GFP expression patterns of the medaka *fli1*-GFP transgenic line after ventricular resection. A–D: Fluorescent images of hearts of the *fli1*-GFP transgenic line: uncut heart (A) and resected hearts at 4 dpa (B), 7 dpa (C), and 14 dpa (D). Infiltration of the wound site by GFP-positive cells was not observed by 14 dpa (D). The dashed line indicates the approximate injury border. myo, myocardium; wo, wound area. PI, propidium iodide.

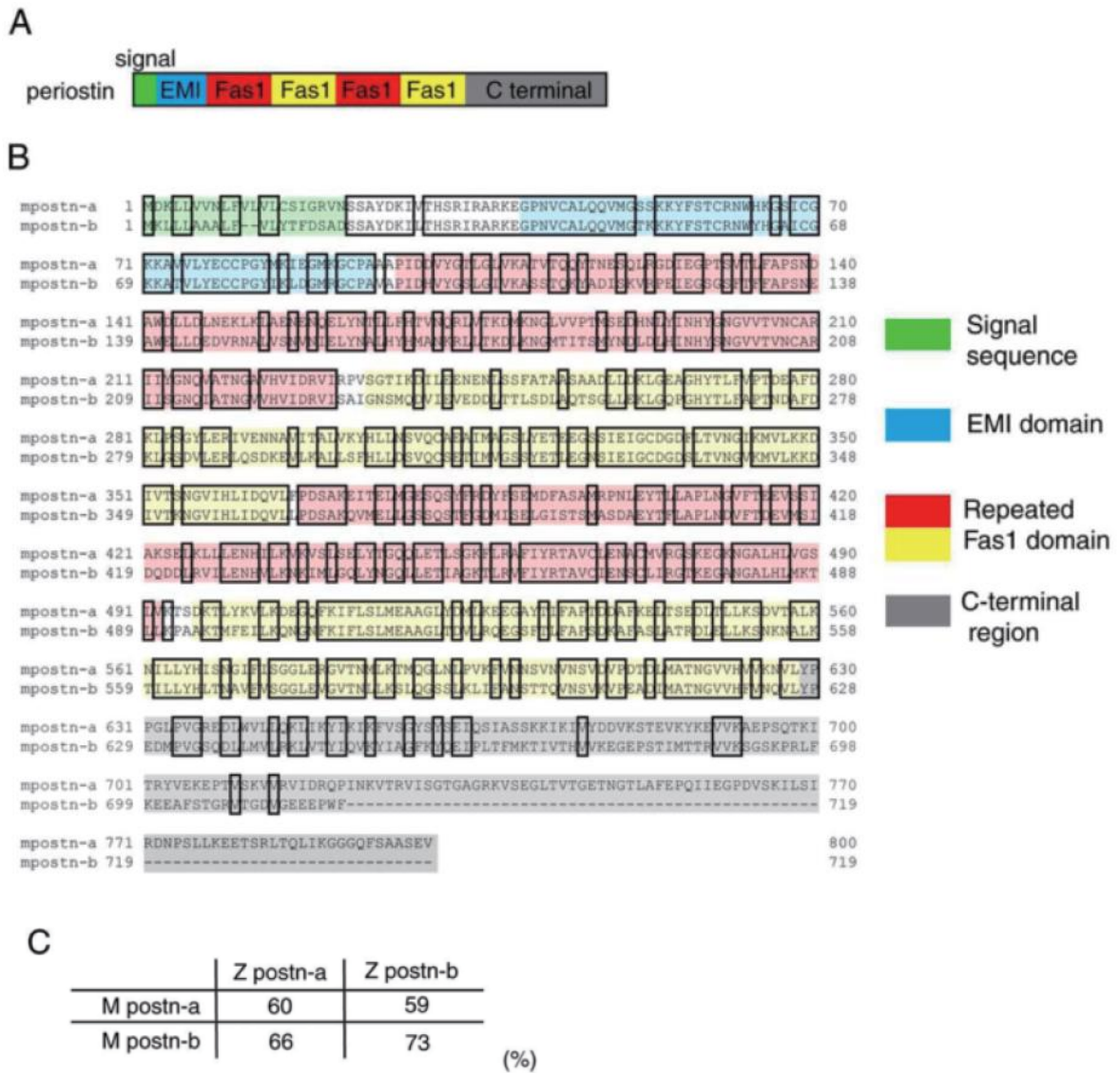


Fig. 1-10. Structure, sequence, and homology of medaka periostin.

(A) The protein structure of periostin.

(B) The conserved amino acid sequences are emphasized by rectangles. The different domains are highlighted by each color code, consistent with the colors in “A” (green, signal sequence; blue, EMI domain; red and yellow; tandemly repeated Fas1 domains; gray, C-terminal region). mpostn, medaka periostin.

(C) Amino acid conservation (%) for each fish periostin protein (M, medaka; Z, zebrafish).

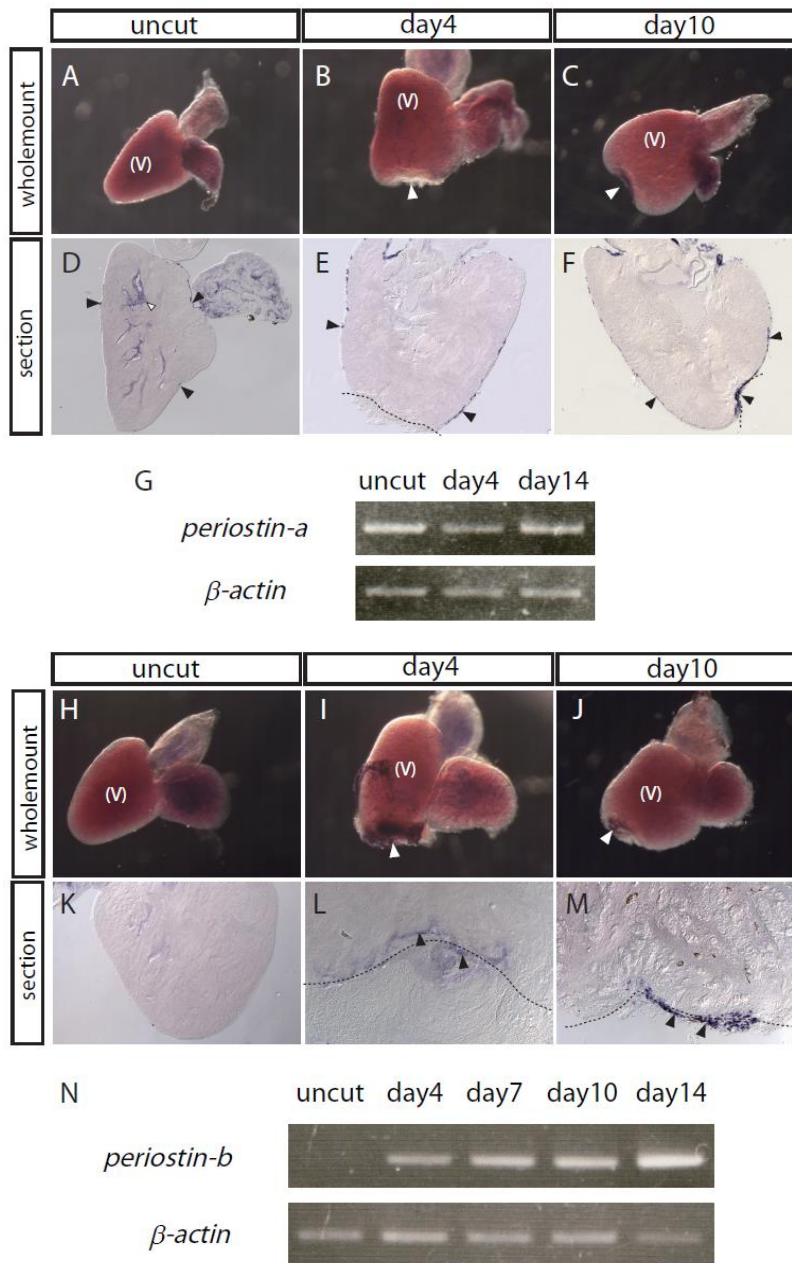


Fig. 1-11. Expression pattern of medaka *periostins* after ventricular injury.

A-F: In situ hybridization analysis of *periostin-a* in uncut (A, D), 4 day (B,E) and day 10 (C,F) hearts.

(G) A semi-quantitative PCR analysis of *periostin-a*.

H-M: In situ hybridization analysis of *periostin-b* in uncut (H, K), 4 day (I, L) and day 10 (J, M) hearts.

(N) A semi-quantitative PCR analysis of *periostin-b*.

Arrowheads indicate *periostin* expression. Black dashed line indicates amputation line.

V. ventricle.

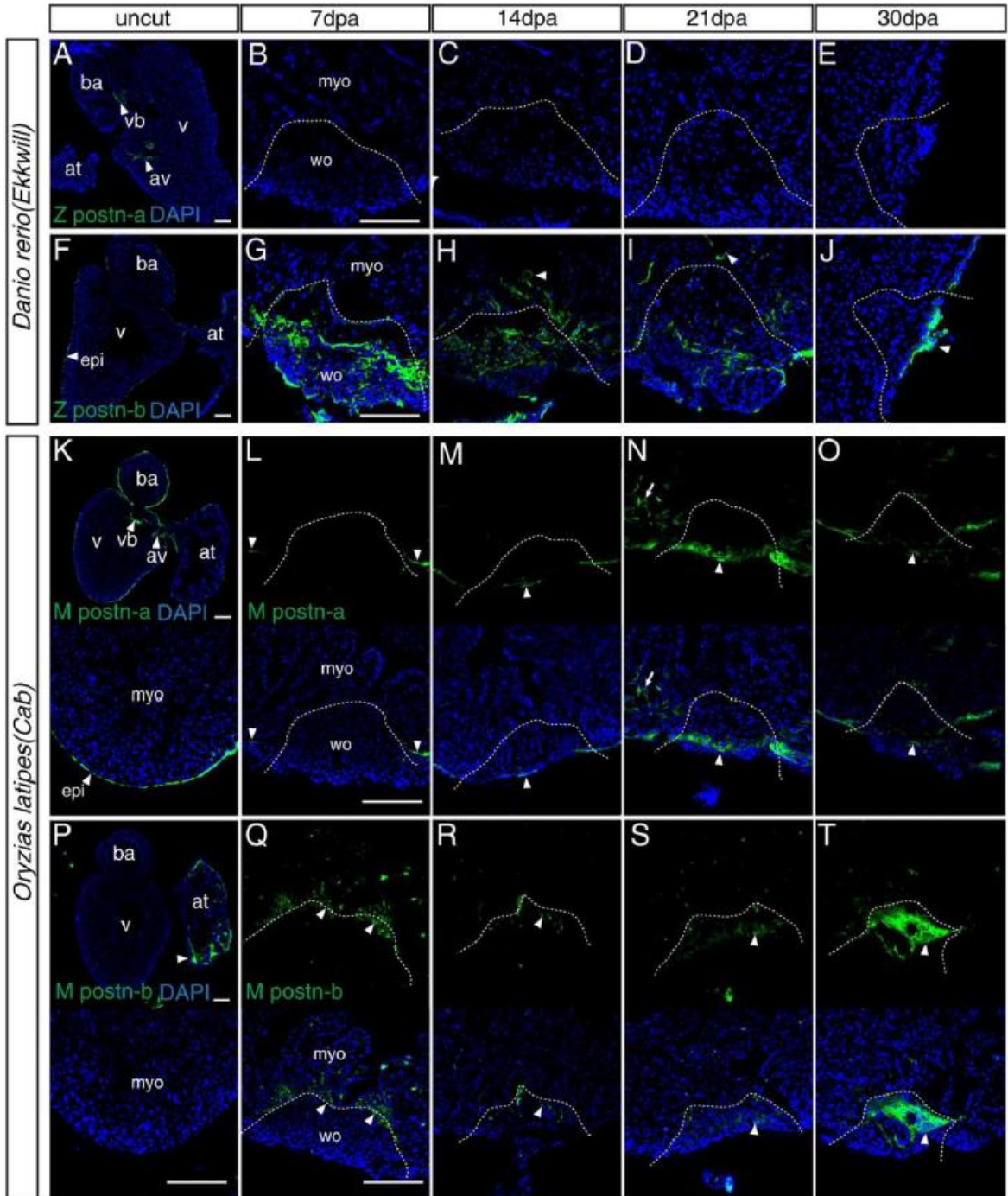


Fig. 1-12. Periostin localization patterns in zebrafish and medaka injured hearts.

A–J: Zebrafish hearts immunostained with anti-zebrafish periostin antibodies.

K–T: Medaka hearts immunostained with anti-medaka periostin antibodies.

A–E: Zebrafish periostin-a localization patterns. Periostin-a was localized at atrio-ventricular (av) valves and ventriculo-bulbal (vb) valves in the uncut heart (A). No localization was observed in the wound

after resection (B–E). F–J: Zebrafish periostin-b localization patterns. Periostin-b was localized in the epicardium and valves (data not shown) in the uncut heart (F). The localization was observed at the wound site at 7 dpa (G), 14 dpa (H), and 21 dpa (I). Endocardial localization was detected at 14 dpa (H, arrowhead) and 21 dpa (I, arrowhead). The localization was restricted to the epicardium by 30 dpa (J, arrowhead).

K–O: Medaka periostin-a localization patterns. Periostin-a localization was observed in the epicardium and valves in the uncut heart (K). The localization was observed in the epicardium during repair (L–O), and its expression seemed to cover the wound. The signal was also observed in the endocardium occasionally (N, white arrow).

P–T: Medaka periostin-b localization patterns. Periostin-b was localized in the atrium (P) and valves (data not shown). The localization was observed at the wound and the injury border from 7 dpa to 30 dpa (Q–T).

Z postn, zebrafish periostin; M postn, medaka periostin. Arrowheads indicate periostin localization. The dashed line indicates the approximate injury border. at, atrium; av, atrio-ventricular valves; ba, bulbus arteriosus; epi, epicardium; myo, myocardium; v, ventricle; vb, ventriculo-bulbal valves; wo, wound area. Scale bars = 100 μ m.

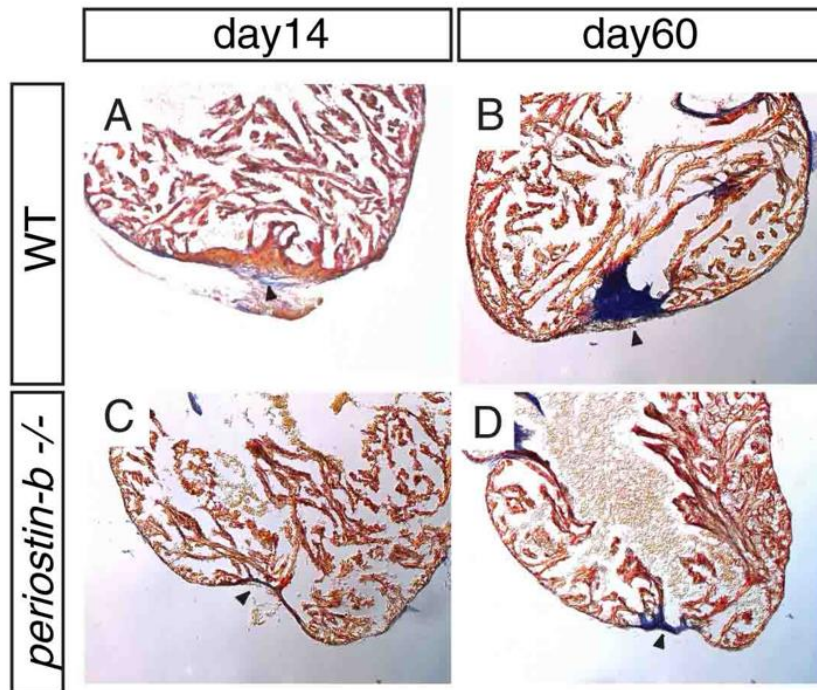


Fig. 1-13. Reparative phenotype in *periostin-b* mutant heart after injury. AFOG staining images of wild type (A, B) and *periostin-b* mutant (C, D). Arrowheads indicate collagen scar.

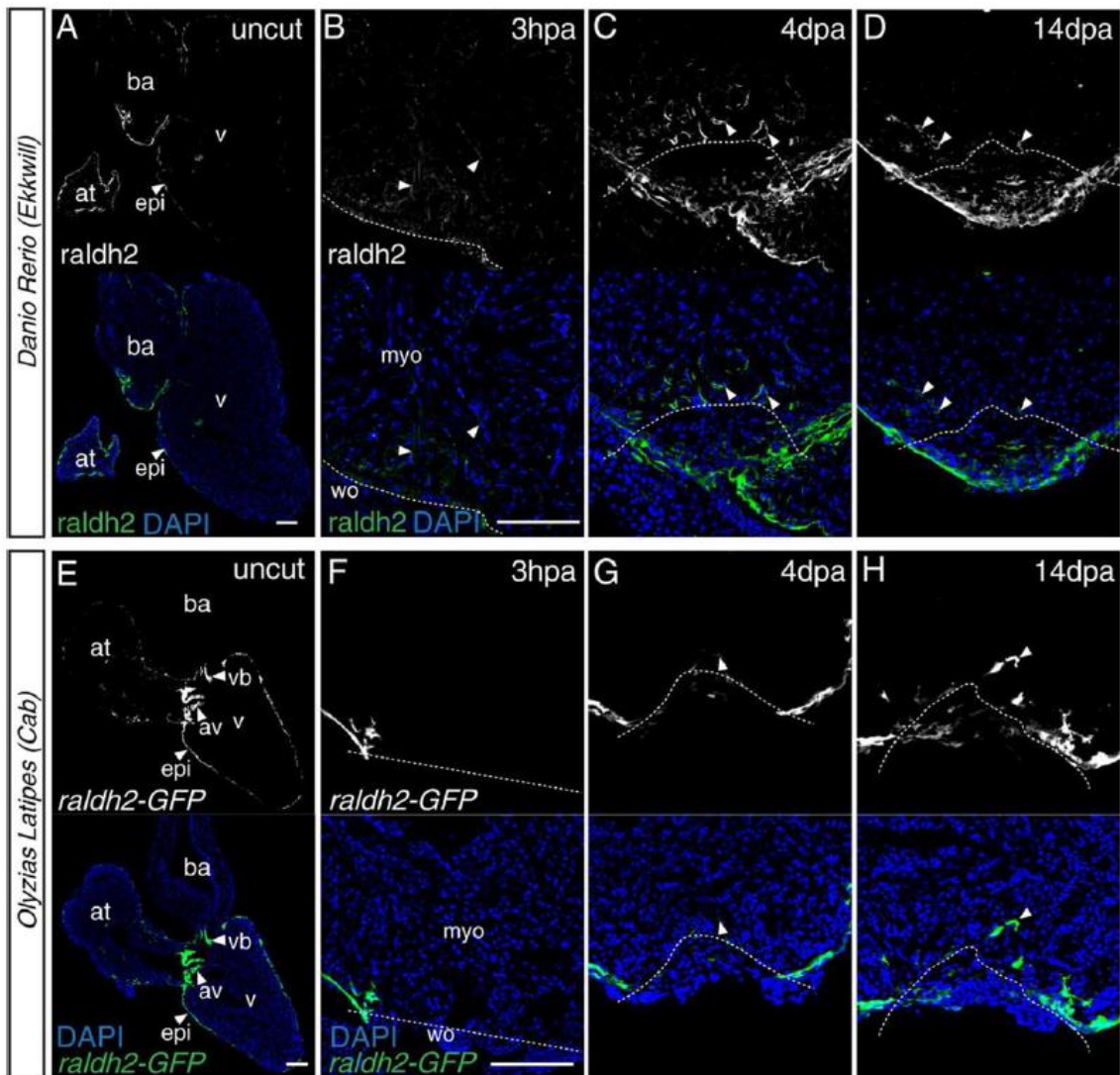


Fig. 1-14. Raldh2 analysis after ventricular resection.

A–D: Fluorescent images of immunostaining for raldh2 in the zebrafish heart (black-white images in the upper row). Raldh2 localization was observed in the epicardium of the uncut heart (A). At 3 hpa (hours post-amputation), endocardial localization of raldh2 was observed (B). Endocardial localization was strengthened and retained at 4 dpa (C) and 14 dpa (D). Raldh2 localization was also observed at the wound site at 4 dpa (C) and 14 dpa (D).

E–H: Fluorescent images of heart of the medaka raldh2-GFP transgenic line (black-white images in the upper row). Raldh2 expression was observed in the epicardium of the uncut heart (E). At 3 hpa, only epicardial expression was observed (F). Raldh2-GFP positive fibroblast-like cells were observed in the wound and myocardial area at 4 dpa (G) and 14 dpa (H), whereas no endocardial raldh2 expression was observed. Arrowheads indicate the raldh2 expression or localization. The dashed line indicates the approximate injury border. at, atrium; av, atrio-ventricular valves; ba, bulbus arteriosus; epi, epicardium; myo, myocardium; v, ventricle; vb, ventriculo-bulbal valves; wo, wound area. Scale bars =100 μ m.

Chapter 2 Proliferation/ hypertrophy transition of neonatal cardiomyocytes and retinoic acid

2-1. Introduction

The heart is an essential organ that works throughout life of animals. The cardiac development is carried out through a series of complicated and delicate processes. An early cardiac development has been drawing many researchers' attention because cardiac abnormalities in embryonic stages lead to death in many cases. On the other hand, however, postnatal cardiac development, especially at the neonatal development stage have not been fully explored. Hearts experience drastic change of circumstances just after birth such as an exposure to abundant oxygen. An oxidative stress induces DNA damage in CM, leading to cell cycle arrest for genome protection^{49,50}. While CMs stop proliferation, hearts have to manage elevation of the blood pressure associated with body growth. To meet this demand, postnatal hearts are known to increase their capacity for pressure by hypertrophy of individual CMs (Fig. 2-1). This growth-associated hypertrophy is called physiological hypertrophy to discriminate from pathological hypertrophy used in disease context. A mechanism which regulates these neonatal proliferation/ hypertrophy transition is unknown.

As mentioned in general introduction, RA is implicated in hypertrophy and proliferation of CM, and the role of RA in the neonatal proliferation/ hypertrophy transition has not been investigated. Therefore, the author explored the relationships between RA and neonatal maturation in mice in this study.

2-2. Materials and Methods

Mouse

The Jcl:ICR mouse line was used in all experiments in this chapter. Experiments were conducted according to protocols approved by the Institutional Animal Care and Use committee of IMCB, the University of Tokyo.

RNA isolation, cDNA synthesis and Quantitative PCR

Sacrificed hearts were homogenized by Biomasher II (Nippi) with Sepasol (Nacalai Tesque). Total RNA was extracted by phenol- chloroform method, and purified by NucleoSpin RNA (Takara). Then cDNA was synthesized with 1 µg RNA template by using ReverTra Ace qPCR RT Master Mix (TOYOBO).

Quantitative PCR was performed with Thermal Cycler Dice Real Time System II (Takara). Primer pairs used in qPCR were as follows:

Raldh1: F-ATACTTGTCGGATTTAGGAGGC

R-GGGCCTATCTTCCAAATGAACA

Raldh2: F-CAGAGAGTGGGAGACTGTTCC

R-CACACAGAACCAAGAGAGAAGG

Raldh3: F-GGGTCACACTGGAGCTAGGA

R-CTGGCCTCTTCTTGGCGAA

RAR α : F-ATGTACGAGAGTGTGGAAGTCG

R-ACAGGCCCGGTTCTGGTTA

RAR β : F-CTGCTCAATCCATCGAGACAC

R-CTTGTCTTGGCAAACGAAGC

RAR γ : F-GGAGCAGGCTTCCCATTTCG

R-CATGGCTTATAGACCCGAGGA

Cyp26a1: F-AAGCTCTGGGACCTGTACTGT

R-CTCCGCTGAAGCACCATCT

Cyp26b1: F-TCATCGGAGAGACTGGTCACT

R-GGTGCTCACTAGCTGGTGTTTC

Nppa: F-TGACAGGATTGGAGCCCAGAG

R-AGCTGCGTGACACACCACA

Nppb: F-AGTCCTTCGGTCTCAAGGCA

R-CCGATCCGGTCTATCTTGTGC

Histology

Immunohistochemistry was performed on hearts fixed in 4% PFA (2x overnight 4°C) and washed in PBS. Hearts were embedded into frozen block and sliced at 5 µm thickness. Frozen sections were blocked (PBS, 5% Blocking One Reagent (Nakalai Tesque)) for 30 minutes followed by incubation (in block) with primary antibody at 4°C overnight. Slides were then washed in PBS three times for 10 minutes each. Sections were incubated 2 hours with secondary antibody in block followed by washing (3x 10 min) in PBS and then mounted with Prolong Gold Antifade Reagent (Thermo Fisher Scientific).

Primary antibodies (Ab) used were as follows: Anti-MEF2 Ab (Santacruz) at 1:50, Anti-Raldh2 Ab (Sigma) at 1:500, Anti-Raldh1 Ab (Millipore) at 1:400, Anti-Raldh3 (GENETEX) at 1:400, Anti-TroponinT Ab (Thermo fisher scientific) at 1:200, Anti-GFP Ab (MBL) at 1:500, Anti-CD31 Ab (Abcam) at 1:50, Anti-Vimentin (Novus Biologicals) at 1:500.

Secondary antibodies used were AlexaFluor 488/594 (Thermo Fisher Scientific) at

1:1000. DAPI was mixed in secondary antibody solution at 1:1000.

HE staining and Masson's Trichrome staining were carried out as described previously⁵¹.

EdU staining in frozen section was carried out according to manufacturer's instruction.

ALDEFLUOR assay

Sacrificed hearts were torn into small pieces by using forceps, in HBSS solution. Then pieces were enzymatically dissociated by Pierce Primary Cardiomyocyte Isolation Kit (Thermo Fisher Scientific). The dissociation protocol follows manufacturer's instruction. Dissociated cells were incubated 30 minutes with ALDEFLUOR reagent at 37 °C. Negative control was prepared with DEAB (Raldh inhibitor)-added ALDEFLUOR solution. Incubated cells were then analyzed and sorted by FACS Aria-II (BD Biosciences). For immunocytochemistry, sorted cells were mounted to slides by using Cytospin4 cytocentrifugator (Thermo Fisher Scientific).

All-trans RA/ DEAB treatment and EdU incorporation

In RA treatment, 0.3 µg/g of All-trans RA (Sigma aldrich) in corn oil was injected into P2 neonatal abdominal cavity. The injection was carried out daily until sacrifice at P8. As a negative control, DMSO in corn oil was injected into control mice. At P8, 0.2 mg/ g of EdU in saline was also injected intraperitoneally and incubated 30 minutes before sacrifice.

In DEAB treatment, 0.1 mg/ g of diethylaminobenzaldehyde (DEAB, Sigma aldrich) in corn oil was injected intraperitoneally into neonates. All the other procedures were carried out as same as RA treatment.

2-3. Results

2-3-1. CM proliferation and hypertrophy after birth.

At first, the author has tried to reproduce previous results reported so far. Many studies have reported that drastic cell cycle arrest occurs in CM at neonatal stages^{49,50}. To confirm the decrease of CM proliferation, the author conducted EdU incorporation into neonatal mice and examined ratio of proliferating CMs in ventricle by counting EdU⁺ MEF2⁺ cells/total MEF2⁺ cells (Fig. 2-2A). MEF2 (Myocyte Enhancer Factor 2) is a myocyte-specific transcription factor which marks CM nuclei in heart. As the results previously reported, the ratio of proliferating CMs was rapidly decreased until 2 weeks after birth. At postnatal day 14 (P14), EdU⁺/MEF2⁻ mesenchymal cells were also few, while they were actively proliferating at postnatal day 1.

As mentioned above, initiation and progression of physiological CM hypertrophy instead of CM proliferation is a well-known event during postnatal cardiac maturation⁵². The author confirmed postnatal expression of hypertrophy markers, *Nppa* and *Nppb*, the hormones secreted in response to cardiac stresses (Fig.2-2B). Both markers were gradually upregulated from birth to adult stage, implicating increase in cardiac stresses accompanying CM hypertrophy.

The CM proliferation was almost terminated at P14, indicating that the transition ends until P14. Therefore, the author focused on first 2 weeks after birth in subsequent experiments.

2-3-2. Transient upregulation of *Raldh2* in neonatal hearts.

To explore the relationship between RA and neonatal cardiac maturation, the author examined neonatal expression of three retinaldehyde dehydrogenases (*Raldhs*) *Raldh1*, *Raldh2* and *Raldh3* that efficiently oxidize retinaldehyde into RA⁵³⁻⁵⁵. Of three genes, *Raldh2* was transiently upregulated at higher levels than the other (Fig. 2-3A). *Raldh2* expression peaked at P7 and was diminished thereafter. *Raldh1* expression was also increased after birth and the peak was P21, but *Raldh3* expression was kept at low levels throughout the period. These results suggest the significance of *Raldh2* during the proliferation/ hypertrophy transition of CM that occurs 2 weeks after birth.

To ensure the results of the expression analysis, the author investigated localization of each enzyme in neonatal hearts (Fig.2-3B). Immunohistochemical analysis revealed that *Raldh2* localizes at the epicardium and many interstitial cells adjacent to CMs. In contrast, *Raldh1* localization was restricted to the epicardium. As for *Raldh3*, the localization could not be detected. Furthermore, the interstitial *Raldh2* localization disappeared by 2 weeks after birth (Fig. 2-3C), and the localization was not detected in adult hearts (Fig. 2-3D).

From these results, interstitial *Raldh2*⁺ cells seem to work transiently during neonatal stages.

2-3-3. Transient increase of RA synthetic cells in neonatal hearts

As the expression and localization of Raldh enzymes are indirect evidence of RA synthesis, the author examined Raldh enzymatic activity in neonatal hearts by ALDEFLUOR assay. ALDEFLUOR substrate is metabolized by active Raldh enzymes and the metabolized products exhibit fluorescence (Fig. 2-4A). The fluorescence in individual cells can be detected by using FACS. In neonatal stages, the ratio of Raldh-active cells was kept at high levels, and peaked at P7 and decreased thereafter, which is consistent with *Raldh* expression analysis (Fig.2-4B). These results indicate that the enzymatic activity in hearts was elevated in association with the upregulation of *Raldh* genes.

2-3-4. Expression analysis of RA-relative genes.

To further support RA production in neonatal hearts, the author investigated the expression pattern of nuclear RA receptor *RARs* (*RAR α* , *RAR β* , *RAR γ*)^{56,57} (Fig. 2-5A) and RA metabolizing enzyme *Cyp26s* (*Cyp26a1*, *Cyp26b1*)^{8,58} (Fig. 2-5B). As a result, *RAR α* and *RAR β* mRNA were increased during neonatal stages and they peaked at P7. *RAR γ* mRNA was slightly increased after birth, but there was no notable change until the adult stage. *Cyp26a1* mRNA was increased in neonatal hearts but the peak was P4, earlier than the peak of *Raldhs* or *RARs*, which implies a quick response to RA increase.

These results suggest the neonatal activation of the RA signaling pathways in RA-responsive cells.

2-3-5. Cell type analysis of Raldh2⁺ cells.

If the activation of the RA-response pathway was not induced by RA in blood stream, the cardiac interstitial Raldh2⁺ cells can be considered a main resource of RA in neonatal heart. However, as the properties of Raldh2⁺ cells is unknown, the author examined whether Raldh2⁺ cells are cardiac muscle or not by using the transgenic mouse line expressing GFP by the *Myh6* promoter. *Myh6* encodes myosin heavy chain 6 and has been used as a CM marker⁵⁹. Co-immunohistochemistry of Raldh2 with GFP (Fig. 2-6A) revealed that Raldh2 and GFP were not merged. Moreover, Raldh2 was not merged with another CM marker, TroponinT (Fig. 2-6B). Next, the author tried to co-immunostaining with CD31, a marker for endocardial epithelial cells but was not co-localized with Raldh2 (Fig. 2-6C).

Finally Raldh2 was found to co-localize with Vimentin, a fibroblast marker (Fig.2-6D). Co-immunostaining against isolated cardiac fibroblasts revealed that all fibroblasts were Raldh2⁺ (Fig. 2-6E). Furthermore, ALDEFLUOR⁺ cells sorted by FACS were all Vimentin⁺ (Fig. 2-6F). These results based on *Raldh2* expression indicate that Raldh2⁺ cells are fibroblastic and neonatal cardiac fibroblasts are a homogenous population.

2-3-6. *In vivo* effects of all-trans RA in neonatal mice.

To examine the function of RA in neonatal hearts, the author investigated cardiac phenotype under RA-excessive condition by intraperitoneal injection of all-trans RA (Fig. 2-7A). As a result, the body and heart under the RA-excessive condition grew well compared with DMSO-injected control mice (Fig. 2-7B). HW/ BW of RA-injected mice was also elevated (Fig. 2-7C). In these hearts, *RARs* were upregulated (Fig. 2-7D), which is indicative of excessive activation of RA signaling in RA-injected mice. Of three *RARs*, *RAR β* mRNA was significantly increased in response to exogenous RA, which was consistent with the results of expression analysis in normal neonatal hearts (Fig. 2-5A).

The author then examined whether these cardiac phenotypes were induced by CM proliferation or CM hypertrophy. In RA-excessive mice, the ratio of proliferating CM was significantly increased (Fig. 2-7E). On the other hand, *Nppa* and *Nppb* mRNA expressions were attenuated in RA-excessive mice, indicative of a decrease of cardiac stresses and accompanying CM hypertrophy. These results suggest that the cardiac overgrowth phenotype was induced by an increase of CM number as a consequence of CM proliferation rather than CM hypertrophy.

2-3-7. *In vivo* effects of RA synthetic inhibitor (DEAB) in neonatal mice.

Next, the author examined cardiac phenotypes under the RA-deficient condition by injection of diethylaminobenzaldehyde (DEAB) (Fig. 2-8A). DEAB is a commonly used Raldh inhibitor⁶⁰⁻⁶². Contrary to expectations, the DEAB-injected mice showed the same phenotypes as RA-injected mice; body and heart grew well compared with DMSO-injected control mice (Fig. 2-8B). In DEAB-treated mice, CM proliferation was enhanced (Fig. 2-8C). Surprisingly, mRNA of *RARs* were increased by DEAB treatment (Fig. 2-8D), suggestive of the activation of RA signaling. These results suggest that the inhibition of RA synthesis by DEAB might be compensated by unknown mechanisms and thereby RA signaling was activated even greater than control. If the compensation occurred, these phenotypes support the results of RA-excessive condition.

2-4. Discussion

The neonatal stage is a period that individual cells change their characteristic to deal with new circumstances. Such individual changes induce organ-scale alteration and contribute to completion of organogenesis. The cardiac maturation after birth is one of such alteration processes. The author for the first time revealed the relationships between the neonatal cardiac maturation and RA. The expression of RA synthesizing enzyme was transiently upregulated after birth, followed by the expression of the RA-responsive genes. The RA-excessive condition prolonged time window of CM proliferation and induced downregulation of *Nppa* and *Nppb*, the indicator for cardiac stresses. Therefore, one can speculate that RA functions to attenuate cardiac stress at neonatal stages. However, it remains unknown how RA attenuates cardiac stresses. One possibility is that the CM proliferation accelerated by RA contributes to the attenuation because an increase of CM number results in a decrease of pressure load for each CM. Another possibility is that RA directly suppresses the expression of *Nppa* and *Nppb*.

The increase of CM number in neonatal stages may also have a merit for the adult heart. As mentioned above, the arrest of CM cell cycle is an irreversible process, causing cardiac dysfunction in adult pathological conditions. If the heart has the excessive number of CM, the pressure load taken by each CM will become lower levels than in the normal heart, which means that the heart has a high capacity for pathological pressure load. Although the relationship between the neonatal RA level and adult diseased heart is still unknown in this study, further studies with a long-term analysis will clarify that.

The DEAB treatment induced the same phenotype as RA treatment. If a compensation mechanism exists, it implies robustness of RA regulation *in vivo*. Although DEAB is a well-known Raldh inhibitor *in vitro*, there is few papers using DEAB in mice *in vivo*,

which may reflect difficulty of DEAB as an *in vivo* inhibitor. To eliminate RA synthesis *in vivo*, genetic approach such as conditional and multiple knockout of *Raldhs* should be adopted in future.

A mechanism by which RA stimulates CM proliferation is also unknown. Although many studies reported the effects of RA on CM *in vitro*, there is no evidence that RA directly stimulates CM proliferation. Therefore, one can speculate that indirect mechanisms underlie the accelerated CM proliferation by RA injection. If the endogenous RA synthesized in cardiac fibroblasts works in the same manner as exogenous RA, the fibroblasts could be targets of RA to promote CM proliferation via secreting humoral factor such as growth factors or secreting ECM proteins helpful for CM proliferation, and signal transfer to CM via cell membrane. These are possible because similar functions are reported in some papers^{9,10,63-65}.

In conclusion, this study revealed a new role of RA in cardiac maturation and suggested a role of cardiac fibroblasts for stimulating CM proliferation.

2-5. Figures

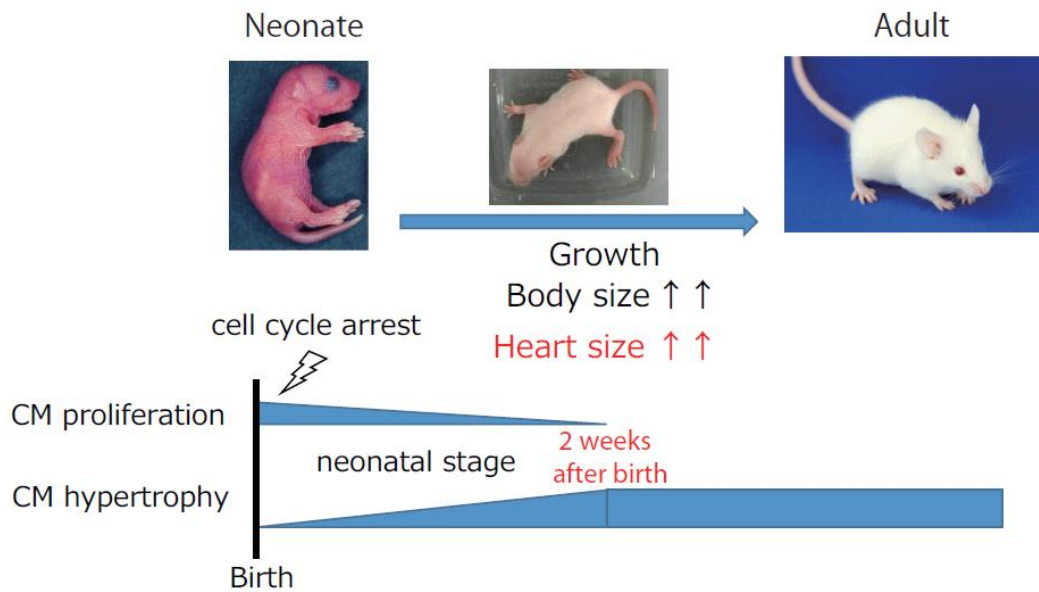


Fig. 2-1. Proliferation/ hypertrophy transition of neonatal cardiomyocytes (CM). Neonatal CMs undergo cell cycle arrest and alternatively heart grows up through CM hypertrophy to meet demands from increasing pressure load associated with body growth.

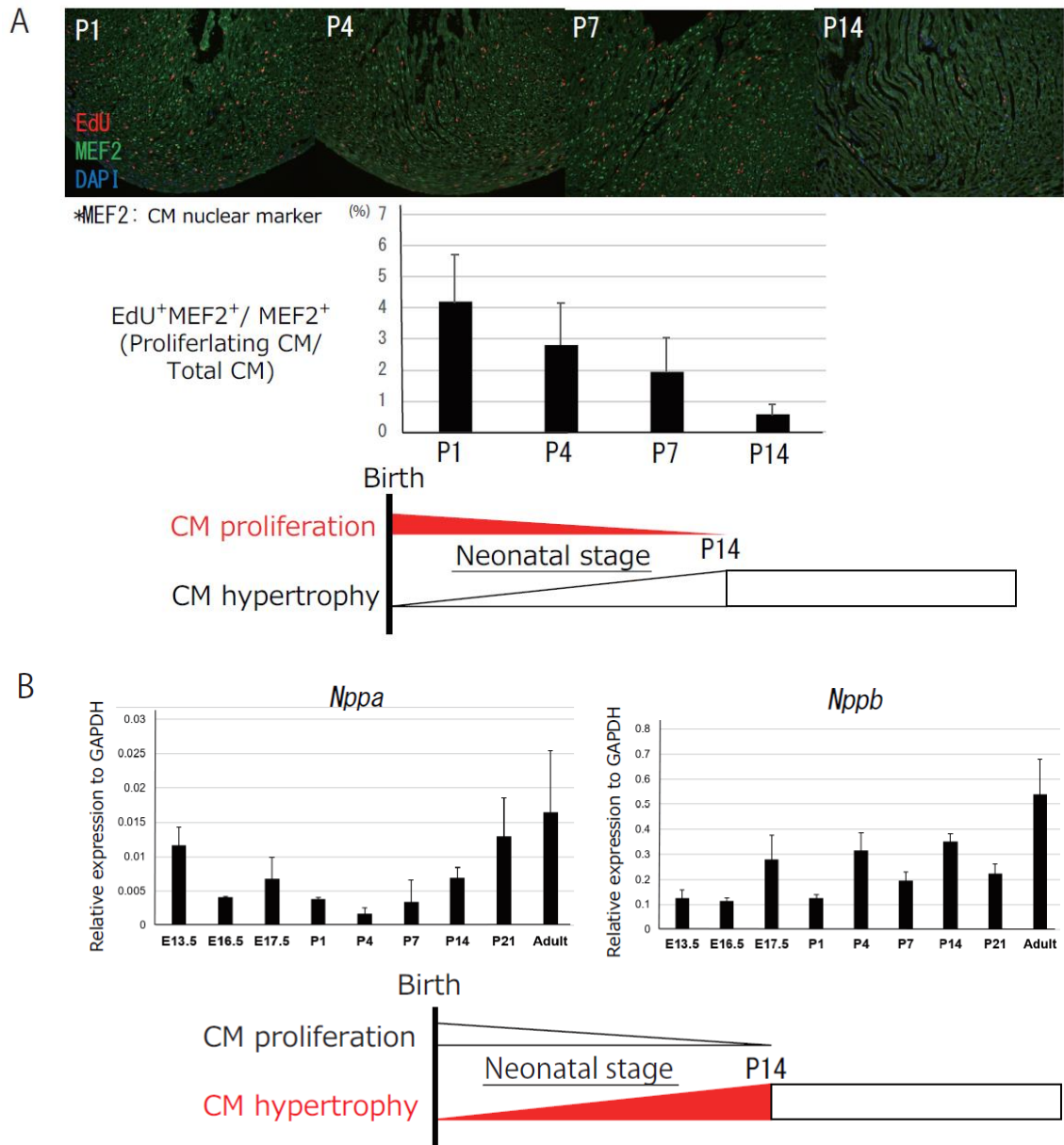


Fig. 2-2. A drastic decrease of CM proliferation and upregulation of hypertrophy marker genes.

(A) Quantification of CM proliferation after birth. n = 4 per group.

(B) Quantitative real time PCR analysis of *Nppa* and *Nppb* genes. n = 4 per group.

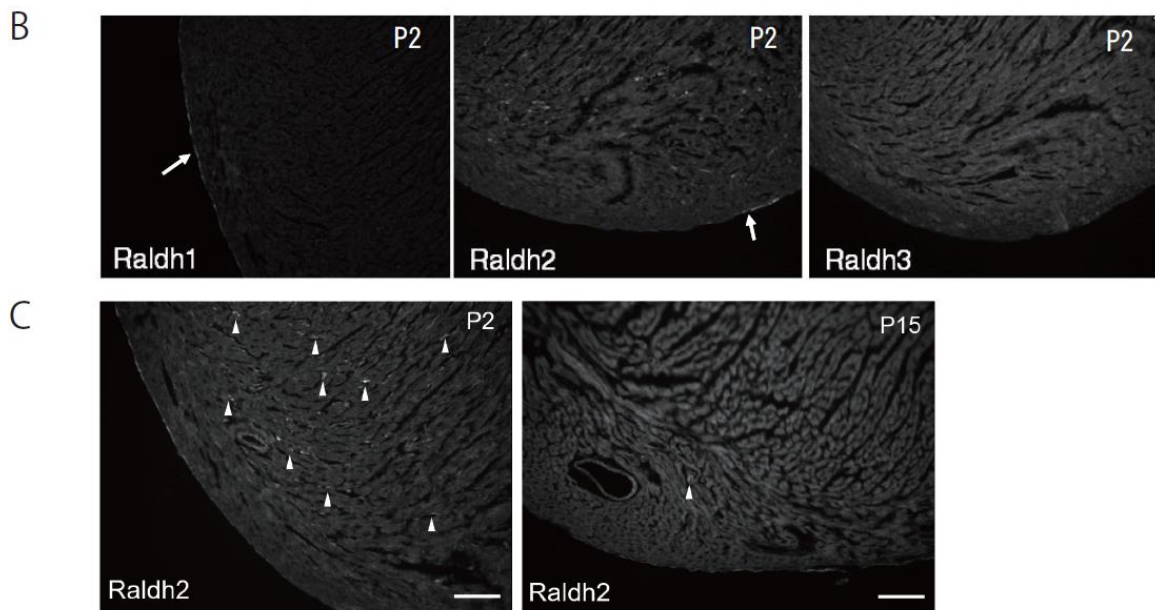
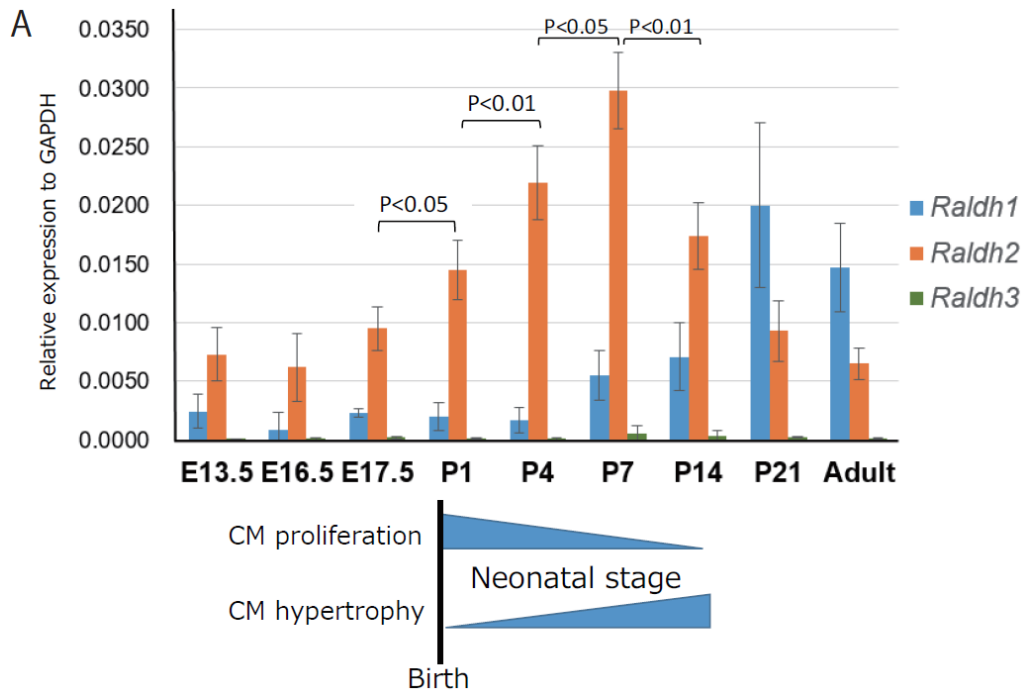


Fig. 2-3. Comparative analysis of Raldh family.

(A) Time series analysis by Quantitative real time PCR of *Raldh1*, *Raldh2* and *Raldh3*.

n = 4 per group.

(B) Immunohistochemistry against Raldh enzymes in P2 heart.

(C) Comparison of Raldh2 localization between P2 and P15 heart.

D

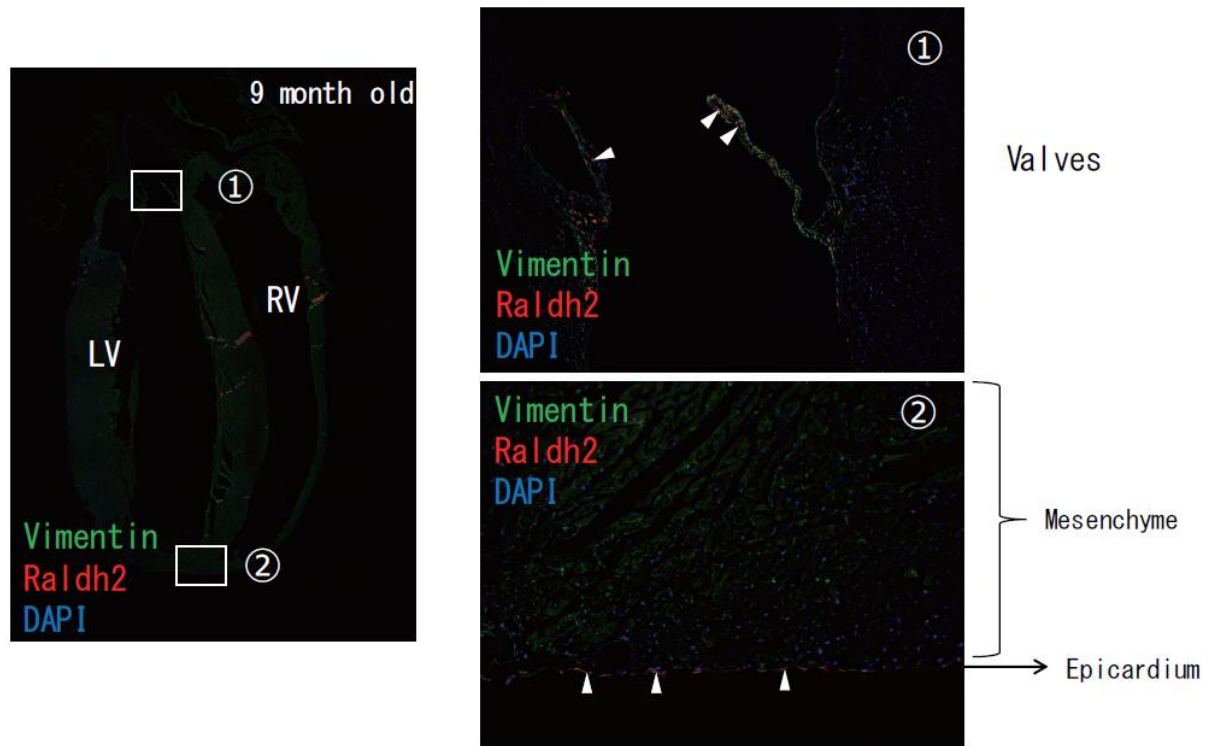


Fig. 2-3. Comparative analysis of Raldh family.

(D) Raldh2 localization in 9 month old heart. Brackets in left figure were magnified in right according to assigned number. Arrowheads indicate Raldh2 localization.

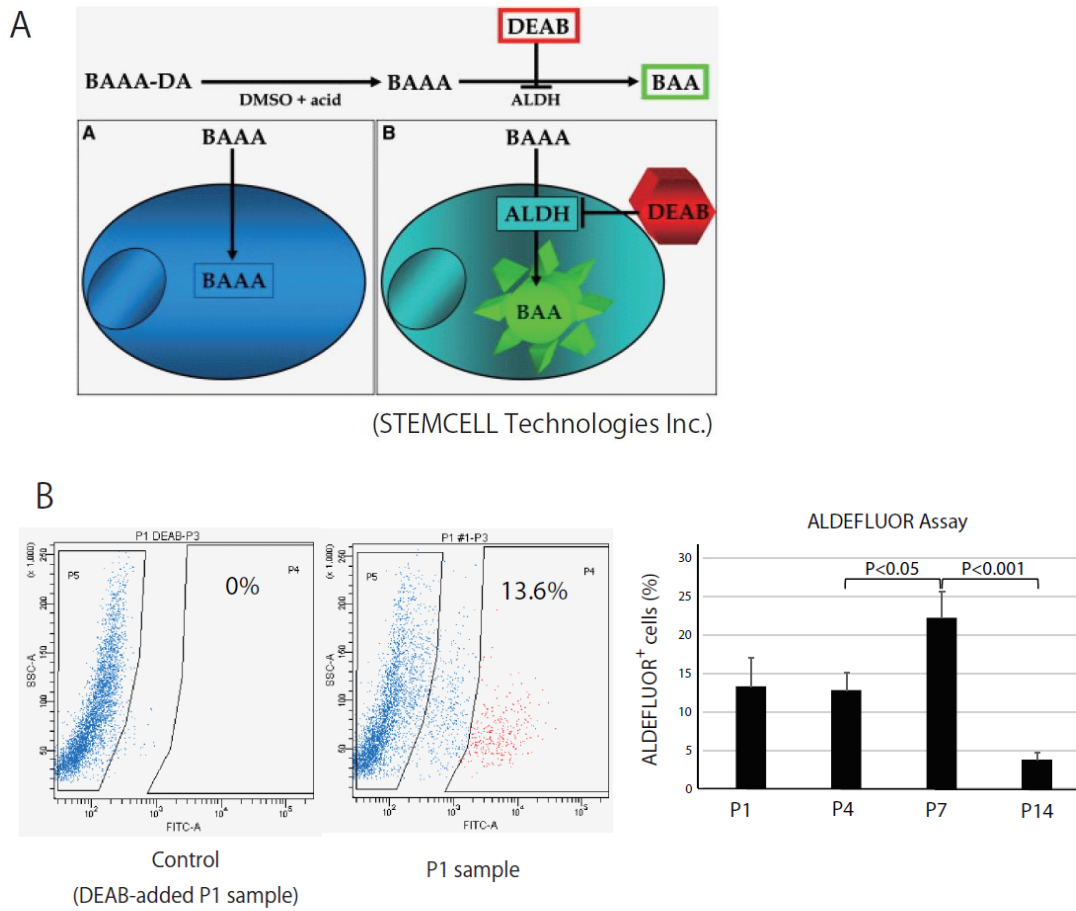


Fig. 2-4. Quantification of cells with RA synthetic activity.

(A) ALDEFLUOR assay. ALDEFLUOR substrates are metabolized by ALDH (Raldhs) and emit fluorescence.

(B) FACS analysis of ALDEFLUOR⁺ cells. Representative results of FACS analysis is shown in left figures. Negative control is prepared by adding DEAB, an inhibitor of Raldhs. Right figure indicates time series analysis of ALDEFLUOR⁺ cells. n = 4 per group.

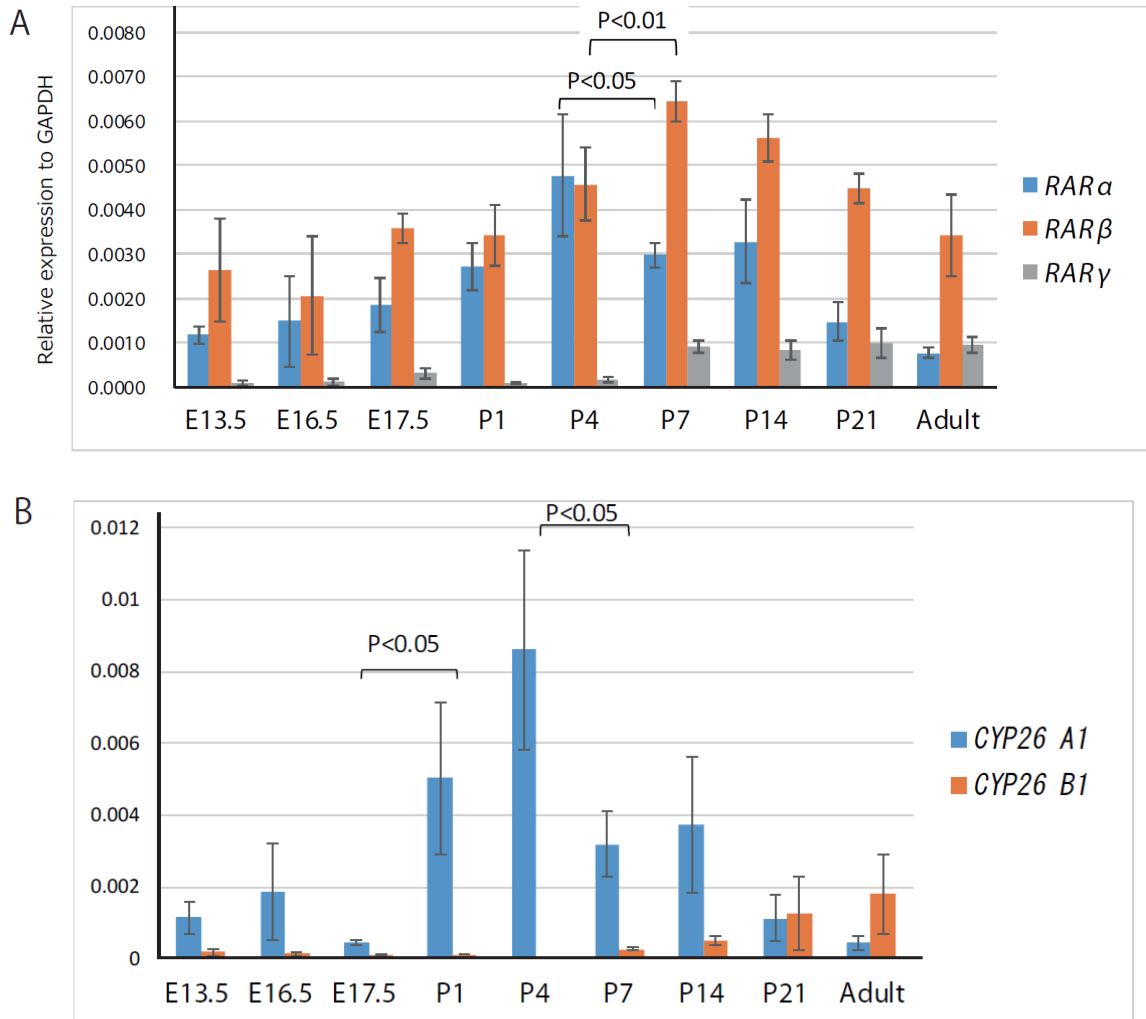


Fig. 2-5. Expression patterns of RA-related genes.

(A) Quantitative real time PCR analysis of RA receptors. n = 4 per group.

(B) Quantitative real time PCR analysis of RA metabolizing enzymes. n = 4 per group.

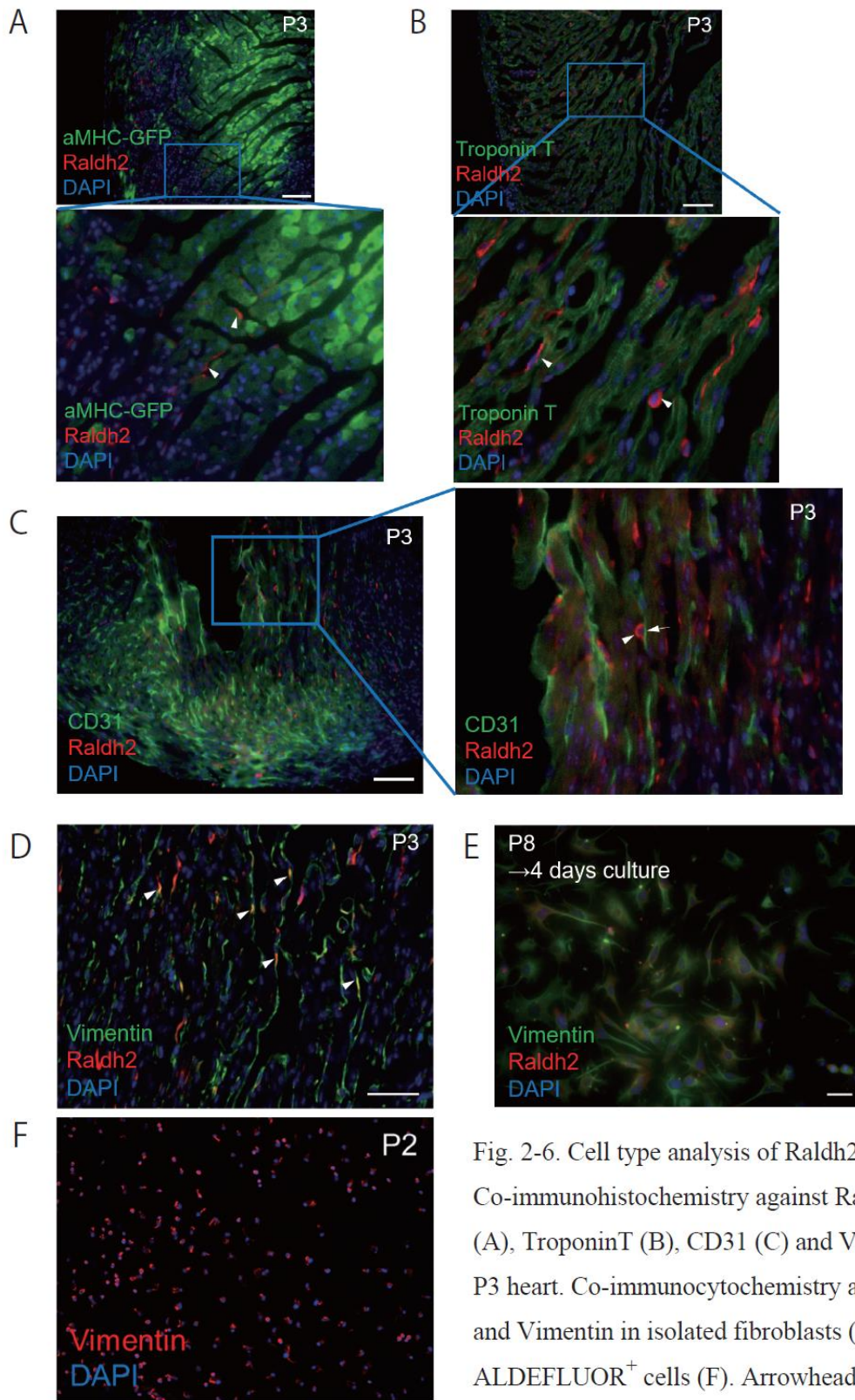


Fig. 2-6. Cell type analysis of Raldh2⁺ cell. Co-immunohistochemistry against Raldh2 and GFP (A), TroponinT (B), CD31 (C) and Vimentin (D) in P3 heart. Co-immunocytochemistry against Raldh2 and Vimentin in isolated fibroblasts (E) and in ALDEFLUOR⁺ cells (F). Arrowheads indicate Raldh2 localization. Arrow in (C) indicates CD31 localization.

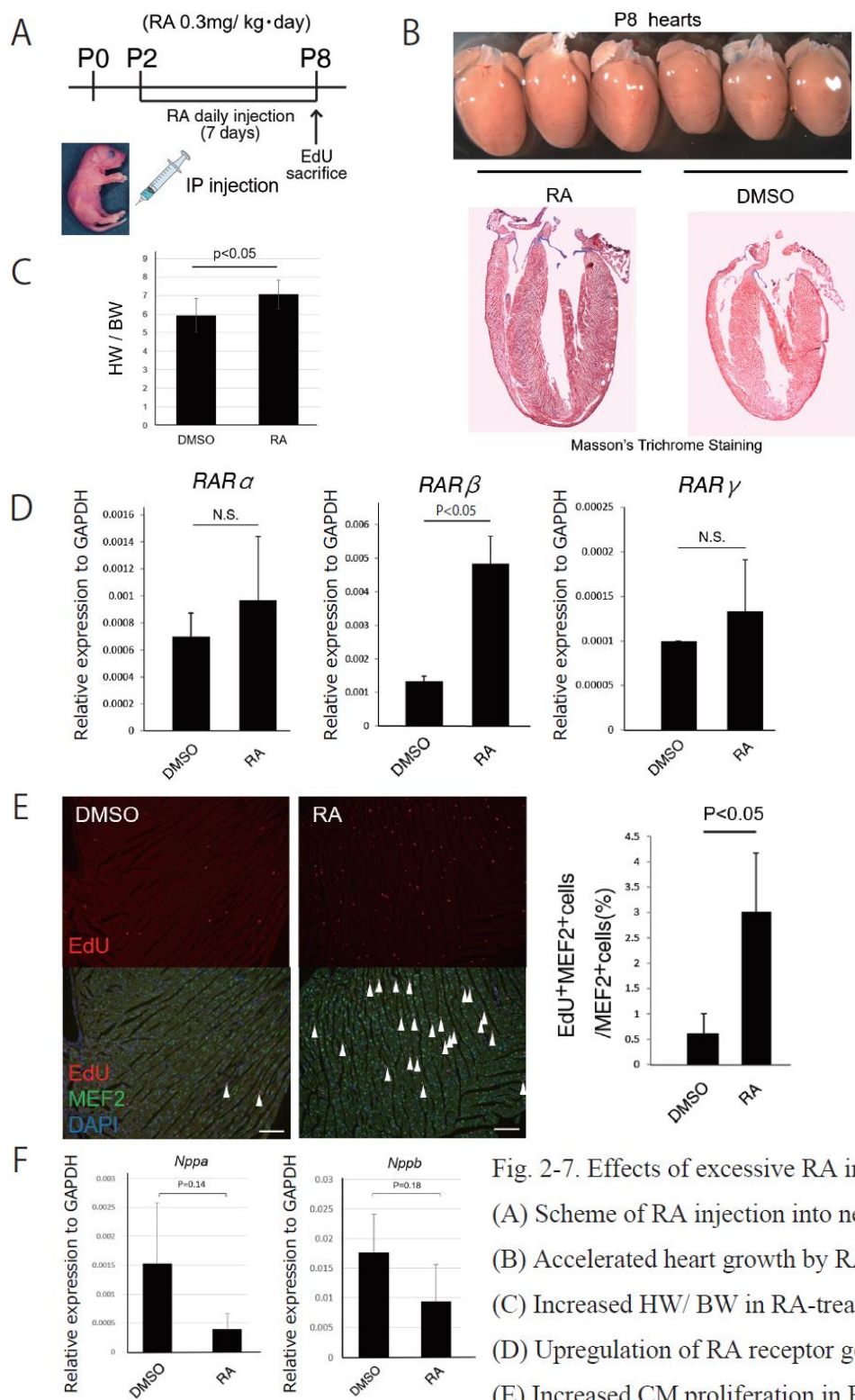


Fig. 2-7. Effects of excessive RA in neonatal heart. (A) Scheme of RA injection into neonatal mice. (B) Accelerated heart growth by RA injection. (C) Increased HW/ BW in RA-treated mice. (D) Upregulation of RA receptor gene expression. (E) Increased CM proliferation in RA-treated mice. (F) Downregulation of *Npp* gene expression. N.S., Not Significant. Arrowheads indicate $\text{EdU}^+\text{MEF2}^+$ cells.

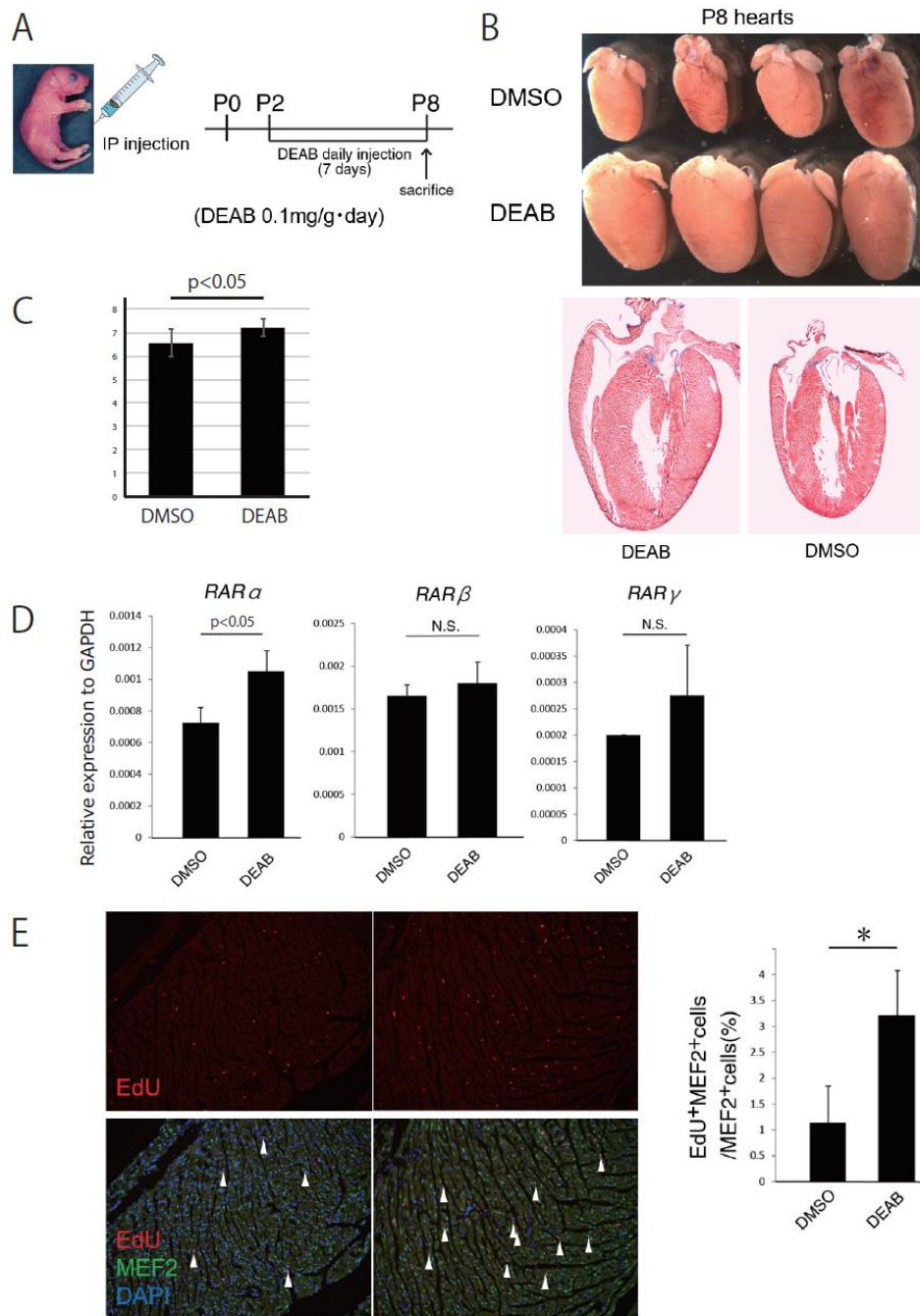


Fig. 2-8. Effects of DEAB in neonatal heart.

(A) Scheme of DEAB injection into neonatal mice.

(B) Accelerated heart growth by DEAB injection.

(C) Increased HW/ BW in DEAB-treated mice.

(D) Upregulation of RA receptor gene expression.

(E) Increased CM proliferation in RA-treated mice.

N.S., Not Significant. Arrowheads indicate EdU⁺MEF2⁺ cells.

Chapter 3 General conclusion

In this study, the author attempted to elucidate functions of retinoic acid in late stage of cardiac development and adult heart regeneration. Based on the results, this study suggests that RA functions not only in early developmental stages but also in heart regeneration and maturation, mainly through stimulating CM proliferation. The study also revealed significant contribution of RA-producing non-CM cells in key events of cardiac development.

The author also found difference in regenerative capacity between fish species for the first time. To investigate differences between regenerative/ non-regenerative fish in detail will help us to understand mechanism of heart regeneration.

These studies will contribute to understand mechanisms underlying later stages of cardiac development and cardiac diseases.

References

1. Niederreither, K., Subbarayan, V., Dolle, P. & Chambon, P. Embryonic retinoic acid synthesis is essential for heart morphogenesis in the mouse. *Nat. Genet.* **21**, 444-448 (1999).
2. Mic, F. A., Haselbeck, R. J., Cuenca, A. E. & Duester, G. Novel retinoic acid generating activities in the neural tube and heart identified by conditional rescue of Raldh2 null mutant mice. *Development* **129**, 2271-82 (2002).
3. Fan, X. *et al.* Targeted disruption of Aldh1l1 (Raldh1) provides evidence for a complex mechanism of retinoic acid synthesis in the developing retina. *Mol. Cell. Biol.* **23**, 4637-4648 (2003).
4. Romand, R. *et al.* Retinoic Acid Deficiency Impairs the Vestibular Function. *J. Neurosci.* **33**, 5856-5866 (2013).
5. He, Y. *et al.* All-trans retinoic acid inhibited angiotensin II-induced increase in cell growth and collagen secretion of neonatal cardiac fibroblasts. *Acta Pharmacol. Sin.* **27**, 423-429 (2006).
6. Zhou, M. D., Sucov, H. M., Evans, R. M. & Chien, K. R. Retinoid-dependent pathways suppress myocardial cell hypertrophy. *Proc. Natl. Acad. Sci. U. S. A.* **92**, 7391-7395 (1995).
7. Wang, H.-J., Zhu, Y.-C. & Yao, T. Effects of all-trans retinoic acid on angiotensin II-induced myocyte hypertrophy. *J. Appl. Physiol.* **92**, 2162-8 (2002).
8. Pan, J. & Baker, K. M. Retinoic Acid and the Heart. *Vitam. Horm.* **75**, 257-283 (2007).
9. Brade, T. *et al.* Retinoic acid stimulates myocardial expansion by induction of hepatic erythropoietin which activates epicardial Igf2. *Development* **138**, 139-148 (2011).
10. Lavine, K. J. *et al.* Endocardial and epicardial derived FGF signals regulate myocardial proliferation and differentiation in vivo. *Dev. Cell* **8**, 85-95 (2005).
11. Kikuchi, K. *et al.* Retinoic acid production by endocardium and epicardium is an injury response essential for zebrafish heart regeneration. **20**, 397-404 (2011).
12. Ma, Y. *et al.* Myofibroblasts and the extracellular matrix network in post-myocardial infarction cardiac remodeling. *Pflugers Arch. Eur. J. Physiol.* **466**, 1113-1127 (2014).
13. Poss, K. D., Wilson, L. G. & Keating, M. T. Heart Regeneration in Zebra sh.

- October* **298**, 2188-2190 (2002).
14. Raya, A. *et al.* Activation of Notch signaling pathway precedes heart regeneration in zebrafish. *Proc. Natl. Acad. Sci. U. S. A.* **100**, 11889-11895 (2003).
 15. Jopling, C. *et al.* Zebrafish heart regeneration occurs by cardiomyocyte dedifferentiation and proliferation. *Nature* **464**, 606-9 (2010).
 16. Kikuchi, K. *et al.* Primary contribution to zebrafish heart regeneration by *gata4(+)* cardiomyocytes. *Nature* **464**, 601-5 (2010).
 17. Gemberling, M., Bailey, T. J., Hyde, D. R. & Poss, K. D. The zebrafish as a model for complex tissue regeneration. *Trends Genet.* **29**, 611-620 (2013).
 18. Lepilina, A. *et al.* A Dynamic Epicardial Injury Response Supports Progenitor Cell Activity during Zebrafish Heart Regeneration. *Cell* **127**, 607-619 (2006).
 19. Kim, J. *et al.* PDGF signaling is required for epicardial function and blood vessel formation in regenerating zebra fi sh hearts. 3-7 (2010).
doi:10.1073/pnas.0915016107/-
/DCSupplemental. www.pnas.org/cgi/doi/10.1073/pnas.0915016107
 20. Mercer, S. E., Odelberg, S. J. & Simon, H. G. A dynamic spatiotemporal extracellular matrix facilitates epicardial-mediated vertebrate heart regeneration. *Dev. Biol.* **382**, 457-469 (2013).
 21. Wang, J., Karra, R., Dickson, A. L. & Poss, K. D. Fibronectin is deposited by injury-activated epicardial cells and is necessary for zebrafish heart regeneration. *Dev. Biol.* **382**, 427-435 (2013).
 22. Horiuchi, K. *et al.* Identification and characterization of a novel protein, periostin, with restricted expression to periosteum and periodontal ligament and increased expression by transforming growth factor beta. *J. Bone Miner. Res.* **14**, 1239-1249 (1999).
 23. Kii, I. *et al.* Incorporation of tenascin-C into the extracellular matrix by periostin underlies an extracellular meshwork architecture. *J. Biol. Chem.* **285**, 2028-2039 (2010).
 24. Kudo, A. Periostin in fibrillogenesis for tissue regeneration: Periostin actions inside and outside the cell. *Cell. Mol. Life Sci.* **68**, 3201-3207 (2011).
 25. Shimazaki, M. *et al.* Periostin is essential for cardiac healing after acute myocardial infarction. *J. Exp. Med.* **205**, 295-303 (2008).
 26. Oka, T. *et al.* Genetic manipulation of periostin expression reveals a role in cardiac hypertrophy and ventricular remodeling. *Circ. Res.* **101**, 313-321

- (2009).
27. Katogi, R. *et al.* Large-scale analysis of the genes involved in fin regeneration and blastema formation in the medaka, *Oryzias latipes*. *Mech. Dev.* **121**, 861-872 (2004).
 28. Loosli, F. *et al.* A genetic screen for mutations affecting embryonic development in medaka fish (*Oryzias latipes*). *Mech. Dev.* **97**, 133-9 (2000).
 29. Naruse, K., Hori, H., Shimizu, N., Kohara, Y. & Takeda, H. Medaka genomics: A bridge between mutant phenotype and gene function. *Mech. Dev.* **121**, 619-628 (2004).
 30. Loosli, F. *et al.* Medaka eyeless is the key factor linking retinal determination and eye growth. *Development* **128**, 4035-4044 (2001).
 31. Nakamura, S., Saito, D. & Tanaka, M. Generation of transgenic medaka using modified bacterial artificial chromosome. *Dev. Growth Differ.* **50**, 415-419 (2008).
 32. Moriyama, A., Inohaya, K., Maruyama, K. & Kudo, A. Bef medaka mutant reveals the essential role of c-myb in both primitive and definitive hematopoiesis. *Dev. Biol.* **345**, 133-143 (2010).
 33. Kudo, H., Amizuka, N., Araki, K., Inohaya, K. & Kudo, A. Zebrafish periostin is required for the adhesion of muscle fiber bundles to the myoseptum and for the differentiation of muscle fibers. *Dev. Biol.* **267**, 473-487 (2004).
 34. Taniguchi, Y. *et al.* Generation of medaka gene knockout models by target-selected mutagenesis. *Genome Biol.* **7**, R116 (2006).
 35. Kamei, Y. *et al.* Development of a convenient in vitro fertilization method using interspecific hybrids between *Oryzias latipes* and *Oryzias curvinotus*. *Dev. Growth Differ.* **49**, 721-730 (2007).
 36. Lien, C. L., Schebesta, M., Makino, S., Weber, G. J. & Keating, M. T. Gene expression analysis of zebrafish heart regeneration. *PLoS Biol.* **4**, 1386-1396 (2006).
 37. Dai, B. *et al.* Reduced collagen deposition in infarcted myocardium facilitates induced pluripotent stem cell engraftment and angiomyogenesis for improvement of left ventricular function. *J. Am. Coll. Cardiol.* **58**, 2118-2127 (2011).
 38. Poss, K. D. Getting to the heart of regeneration in zebrafish. *Semin. Cell Dev. Biol.* **18**, 36-45 (2007).
 39. Brown, L. A. *et al.* Insights into early vasculogenesis revealed by expression of the ETS-domain transcription factor Fli-1 in wild-type and mutant zebrafish embryos. *Mech. Dev.* **90**, 237-252 (2000).

40. Cha, Y. R. & Weinstein, B. M. Visualization and experimental analysis of blood vessel formation using transgenic zebrafish. *Birth Defects Res. C. Embryo Today* **81**, 286-96 (2007).
41. Olivey, H. E., Compton, L. A. & Barnett, J. V. Coronary vessel development: The epicardium delivers. *Trends Cardiovasc. Med.* **14**, 247-251 (2004).
42. Gittenberger-de Groot, A. C. *et al.* The arterial and cardiac epicardium in development, disease and repair. *Differentiation* **84**, 41-53 (2012).
43. Kikuchi, K. *et al.* Tcf21+ Epicardial Cells Adopt Non-Myocardial Fates During Zebrafish Heart Development and Regeneration. *Development* **138**, 2895-2902 (2011).
44. Lemanski, L. F., Fitts, E. P. & Marx, B. S. Fine structure of the heart in the Japanese Medaka, *Oryzias latipes*. *J. Ultrastruct. Res.* **53**, 37-65 (1975).
45. Hu, N., Joseph Yost, H. & Clark, E. B. Cardiac morphology and blood pressure in the adult zebrafish. *Anat. Rec.* **264**, 1-12 (2001).
46. Chablais, F. & Jazwinska, a. The regenerative capacity of the zebrafish heart is dependent on TGF signaling. *Development* **139**, 1921-1930 (2012).
47. Hoover, L. L., Burton, E. G., Brooks, B. a & Kubalak, S. W. The expanding role for retinoid signaling in heart development. *ScientificWorldJournal.* **8**, 194-211 (2008).
48. Porrello, E. R. *et al.* Transient regenerative potential of the neonatal mouse heart. *Science* **331**, 1078-80 (2011).
49. Puente, B. N. *et al.* The oxygen-rich postnatal environment induces cardiomyocyte cell-cycle arrest through DNA damage response. *Cell* **157**, 565-579 (2014).
50. Mahmoud, A. I. *et al.* Meis1 regulates postnatal cardiomyocyte cell cycle arrest. *Nature* **497**, 249-53 (2013).
51. He, L. *et al.* BAF200 is required for heart morphogenesis and coronary artery development. *PLoS One* **9**, 1-8 (2014).
52. Drenckhahn, J. D. *et al.* Impaired myocardial development resulting in neonatal cardiac hypoplasia alters postnatal growth and stress response in the heart. *Cardiovasc. Res.* **106**, 43-54 (2015).
53. Zhao, D. *et al.* Molecular identification of a major retinoic-acid-synthesizing enzyme, a retinaldehyde-specific dehydrogenase. *Eur. J. Biochem.* **240**, 15-22 (1996).
54. Wang, X. *et al.* Cloning of a cDNA Encoding an Aldehyde Dehydrogenase and Its Expression in *Escherichia coli*. *Biochem. J.* **271**, 16288-16293 (1996).

55. Yoshida, A., Rzhetsky, A., Hsu, L. C. & Chang, C. Human aldehyde dehydrogenase gene family. *Eur. J. Biochem.* **251**, 549-57 (1998).
56. Zhang, R., Wang, Y., Li, R. & Chen, G. Transcriptional factors mediating retinoic acid signals in the control of energy metabolism. *Int. J. Mol. Sci.* **16**, 14210-14244 (2015).
57. Through, S., Acid, R., In, R. & Times, R. Signalling Through Retinoic Acid Receptors in Cardiac Development : Doing the Right Things At the. **1849**, 94-111 (2016).
58. Sakai, Y. *et al.* The retinoic acid-inactivating enzyme CYP26 is essential for establishing an uneven distribution of retinoic acid along the anterior-posterior axis within the mouse embryo. *Genes Dev.* **15**, 213-225 (2001).
59. Ishikawa, T. *et al.* Novel mutation in the α -myosin heavy chain gene is associated with sick sinus syndrome. *Circ. Arrhythmia Electrophysiol.* **8**, 400-408 (2015).
60. Morgan, C. A., Parajuli, B., Buchman, C. D., Dria, K. & Hurley, T. D. N,N-diethylaminobenzaldehyde (DEAB) as a substrate and mechanism-based inhibitor for human ALDH isoenzymes. *Chem. Biol. Interact.* **234**, 18-28 (2015).
61. Hamade, A. *et al.* Retinoic acid activates myogenesis in vivo through Fgf8 signalling. *Dev. Biol.* **289**, 127-140 (2006).
62. Mu, X. *et al.* Retinoic acid derived from the fetal ovary initiates meiosis in mouse germ cells. *J. Cell. Physiol.* **228**, 627-639 (2013).
63. Sorrell, M. R. J. & Waxman, J. S. Restraint of Fgf8 signaling by retinoic acid signaling is required for proper heart and forelimb formation. *Dev. Biol.* **358**, 44-55 (2011).
64. Stuckmann, I., Evans, S. & Lassar, A. B. Erythropoietin and retinoic acid, secreted from the epicardium, are required for cardiac myocyte proliferation. *Dev. Biol.* **255**, 334-349 (2003).
65. Ieda, M. *et al.* Cardiac Fibroblasts Regulate Myocardial Proliferation through $\beta 1$ Integrin Signaling. *Dev. Cell* **16**, 233-244 (2009).

Acknowledgement

Firstly, I would like to thank Dr. Jun Takeuchi, Dr. Kazuko Koshihara, Dr. Atsushi Miyajima (IMCB, University of Tokyo) and Dr. Akira Kudo (Tokyo institute of technology) for their assistance and guidance in providing me with the opportunity to be engaged in this research. I also would like to thank all lab members of their laboratories for their helpful advices and experimental assistance. I would like to thank Dr. Tetsu Akiyama (IMCB, University of Tokyo) and Dr. Tetsuya Tabata (IMCB, University of Tokyo) for their assistance of research activity.

I really appreciate Ms. Asuka Miyazawa for her experimental support.

I would like to thank Mrs. Chizuko Koga and Mrs. Nami Otaki for FACS operation.

I would like to thank Dr. Akiko Mantoku, Ms. Mai Morioka and Mr. Taku Akiyama for teaching me basics of research.

Finally, I would like to thank my parents and friends for encouraging me constantly during 6 years of my research life.